Compound Inundation Modeling of a 1-D Idealized Coastal Watershed Using a Reduce-Physics Approach

Félix L. Santiago-Collazo[1], Matthew V. Bilskie[1], Peter Bacopoulos[2], and Scott C. Hagen[2,3,4,†]

[1]School of Environmental, Civil, Agricultural, and Mechanical Engineering, University of Georgia, Athens, GA, USA.
[2]Coastal Ecosystem Design Studio, Louisiana State University, Baton Rouge, LA, USA.
[3]Center for Computation & Technology, Louisiana State University, Baton Rouge, LA, USA.
[4] Department of Civil and Environmental Engineering, Louisiana State University, Baton Rouge, LA, USA.

Corresponding author: Félix L. Santiago-Collazo (fsantiago@uga.edu)

†Deceased

Key Points:

- A reduce-physics flood model was developed to assess compound floods at an idealized coastal watershed transect.
- The magnitude and timing of each flooding mechanism (rainfall-runoff, storm surge, and tides) affect the compound inundation.
- This study may serve as an initial attempt to delineate compound flood hazard zones.

Abstract

Low-gradient coastal watersheds are susceptible to flooding caused by various flows such as rainfall-runoff, astronomical tides, storm surges, and riverine flows. Compound flooding occurs when at least one coastal flood driver occurs simultaneously or in close succession with a pluvial and/or fluvial flood driver, such as during a tropical cyclone event. This study presents a one-dimensional (1-D), reduced-order physics compound inundation model tested over an idealized coastal watershed transect under various forcing conditions (e.g., storm surge, astronomical tides, and rainfall) that varied in magnitude, time, and space. This study aims to evaluate each flooding mechanism and the associated hydrodynamic responses to identify generalized coastal transition zones and enhance the production of flood maps for varying regions in a coastal watershed. Compound inundation levels are affected by the magnitude and timing of each flooding mechanism. The desire is a more holistic compound inundation model that can be a critical tool for decision-makers, stakeholders, and authorities who provide evacuation planning to save human lives and enhance resilience.

Plain Language Summary

Coastal regions with mild sloping terrain can be flooded by intense rainfall, tides, and hurricane storm surges. When multiple flooding events occur at the same location, the inundation effects can be aggravated by the interaction of these physical processes. This study aims to disentangle the complexities of interactive physics according to fundamental concepts. Thus, identifying regions affected by both hydrological and coastal processes can improve flood mapping techniques for coastal communities. Results show that each flood event's strength and time of occurrence affect the total inundation levels. Our research can serve as a foundation for further studies to enhance tools that accurately predict these flood events, resulting in better planning and preparedness for worldwide coastal communities to reduce property damage and loss of lives.

1 Introduction

Coastal watersheds, especially those with low-gradient topography, are under increasing stress due to growing population and infrastructure, frequency of tropical cyclones, sea-level rise, subsidence, and nuisance flooding. Low-gradient coastal watersheds are highly susceptible to flooding caused by various combinations of flows such as rainfall, tides, and storm surge. From 1970 to 2010, the population within US coastal watershed counties increased by 50.9 million (i.e., a 45% increase) to 163.8 million, representing 52% of the entire US population in 2010 (NOAA, 2013). In the decade of the 2010's, 24 billion-dollar (i.e., $1,000 million) weather and climate disaster events occurred within the US, totaling up to $500,000 million (2017 USD) in estimated damages (Lall et al., 2018). Sea level rise and storm surge impacts on coastal properties within the US are projected to be a cumulative cost of $3,600,000 million (2015 USD) by 2100 under a high scenario if no protective measures are implemented (Fleming et al., 2018).

The two most important mechanisms that drive inundation during an extreme meteorological event in a coastal watershed are precipitation (i.e., rainfall) and storm surge. Moreover, waves and astronomical tides mechanisms can enhance the total inundation and, even in some regions, can be the dominating factor. The severity of the inundation from each of these flooding mechanisms can vary due to several factors, such as watershed characteristics (e.g., land use / land cover (LULC), soil type, local bathymetry, and coastal geometry), antecedent

conditions (e.g., soil moisture and initial abstractions), and magnitude of the flood drivers (e.g., duration and intensity of rainfall, intensity and direction of winds, and astronomic tide levels). Therefore, a compound flood event is defined as an inundation event where two or more flooding mechanisms (e.g., riverine flow, rainfall-runoff, storm surge, tides, and waves) from different sources (e.g., pluvial, fluvial, or coastal) co-exist or occur in close succession during a single meteorological event or combination of separate events (Bensi et al., 2020; Bilskie & Hagen, 2018; Bilskie et al., 2021; Blanton et al., 2018; Loveland et al., 2021; Orton et al., 2018; Saleh et al., 2017; Santiago-Collazo et al., 2019; Wahl et al., 2015). Some examples of these meteorological events are tropical cyclones, intense and prolonged rainfall, prevalent strong onshore winds, and low-pressure systems.

Researchers have combined two or more inundation models, statistics, or observed data to quantify compound floods using various coupling techniques since the late 2000s (Santiago-Collazo et al., 2019). However, there has been a heightened urgency to develop detailed two-dimensional (2-D) compound inundation models over the last few years, particularly post-Hurricanes Florence and Harvey (Loveland et al., 2021). For example, there are initiatives to couple the National Water Model (NWM) to coastal inundation models within coastal watersheds (Bakhtyar et al., 2020a; Huang et al., 2021; Tehranirad et al., 2020; Ye et al., 2020; Yin et al., 2021; Zhang et al., 2020). Similarly, the Texas Integrated Flooding Framework is a four-year effort to implement "an integrated framework to model, visualize, and plan for the risk of flooding in counties affected by Hurricane Harvey" (webapps.usgs.gov/tiff/). These initiatives are necessary to advance flood hazard and risk assessments. However, they are still in the research phase, and it will probably take several years to translate research into practical application, especially for national flood hazard mapping. In addition, we must recognize the complexity and challenges associated with floods resulting from disparate driving mechanisms across various spatial and temporal scales. This is the motivation of the work presented herein; to take a step back and simplify the problem by considering a one-dimensional (1-D) approach to compound flood modeling. Findings from this approach will serve as the foundation for future 2-D initiatives by providing insights into the complex interaction of the flooding mechanisms in a compound flood event from its most fundamental physics. In addition, a 1-D model approach is more computationally efficient, thus making it feasible to perform $O(10^3)$ of simulations without a significant computational burden. We recognize the simplifications of a 1-D approach, but such simplifications are often necessary before advancing into additional complexities and degrees of freedom.

This study evaluates the individual flooding mechanisms that can result in a compound flood (i.e., astronomical tides, storm surge, and rainfall-runoff) and the associated hydrodynamic response. An enriched comprehension of the physical interaction of these flooding mechanisms can lead to identifying compound flood hazard zones and, for example, enhance the production of flood maps for varying regions in the coastal watershed. The following study objectives were designed to fill the existing knowledge gaps:

1. Can an idealized domain be created to describe a coastal watershed? To the authors' knowledge, an idealized domain ranging from the inland watershed to the ocean shelf has not been developed. Previous studies have focused on creating idealized ocean domains that do not extend inland and are tested under coastal processes (Dietrich et al., 2005; Mayo et al., 2014; Pandey & Rao, 2019; Veeramony & Blain, 2001). However, there have not been any published attempts regarding idealized inland watershed domains in

the literature. Idealized domains can provide important insights, especially when designing flood protection strategies such as natural infrastructure (Hewageegana et al., 2022).

2. How do current compound flood hazard assessments move beyond traditional (e.g., one- and two-way coupling) approaches toward techniques that fully integrate the flood mechanisms? A reduced-physics, 1-D compound flooding model was developed and used to assess various compound flood scenarios in an idealized domain. Leijnse et al. (2021) is the only published study that uses a similar approach for this purpose. They develop a 2-D model to simulate Hurricane Irma along Florida's northeast coastline. However, their modeling approach utilizes a static boundary condition approach to transfer the coastal processes along the 2-m depth contour of their ocean domain. The proposed study employs a moving boundary condition approach to transfer hydrologic processes into the model. This moving boundary condition is capable of changing the location of the domain where the transfers of hydrologic and coastal processes occur depending on the flood conditions. Therefore, the coupling location and time vary through the different simulations performed. This is the first attempt to develop a spatial and temporally varying reduced physics model in which each node in the domain can change it's governing equation during runtime.

3. Can a compound flood frequency analysis be performed using a physics-based approach rather than based on a statistical one? The vast majority of compound flood models are tested under a single compound inundation event (Bacopoulos et al., 2017; Blanton et al., 2018; Comer et al., 2017; Dresback et al., 2013; Ikeuchi et al., 2017; Lee et al., 2019; Ray et al., 2011; Santiago-Collazo et al., 2017; Wang et al., 2014), whereas others have evaluated up to five compound inundation events (Chen et al., 2013; Chen & Liu, 2014; Van Cooten et al., 2011; Saleh et al., 2017; Torres et al., 2015). However, few studies have conducted hundreds of compound inundation events using the same modeling framework (Zhang & Najafi, 2020). Only one has performed ~1,000 different compound inundation events (Gori et al., 2020b). A compound flood frequency analysis using results from a physics-based modeling approach rather than solely a statistical analysis approach, which is more common in the literature, can be the first step toward a risk assessment of compound floods that estimate annual exceedance probabilities (out-of-scope for this study). This frequency analysis is scarce in the literature due to the high computational cost that demands numerous storm surge and rainfall combinations, especially when using 2-D models (Hsiao et al., 2021). However, to the authors' knowledge, Gori et al. (2020b) is the only peer-reviewed study that developed a frequency analysis to estimate compound flood frequency maps (the model was focused on the Cape Fear, NC watershed). Also, a majority of the literature is based on the coastal-fluvial compound inundation event (Moftakhari et al., 2019; Serafin et al., 2019; Ward et al., 2018), whereas this study is focused on the flood frequency of coastal-pluvial compound inundation event, which is even more scarce in the literature.

4. How crucial is accounting for astronomic tides during a compound flood event? The current literature is limited to compound flood studies that focus only on the dominant processes (i.e., storm surge and rainfall-runoff) brought in a single event, thus neglecting the flooding impacts of the timing of astronomical tides within the compound inundation (Mohanty et al., 2020). For example, only a handful of studies have accounted for the

astronomical tides as part of the coastal process when assessing compound flood by using the dominant tidal constituents in their study region (Gori et al., 2020a; Huang et al., 2021; Leijnse et al., 2021; Mohanty et al., 2020; Ye et al., 2020; Zhang et al., 2020).

A reduced-physics 1-D compound inundation model was developed to bridge these research gaps. This modeling approach simultaneously simulates the free water surface variation in the ocean domain (i.e., tide and storm surge modeling), rainfall-runoff in the watershed's upland region (i.e., hydrology/hydraulic modeling), and compound flooding within the transition zone (Bilskie & Hagen, 2018). A 1-D compound inundation model can run numerous simulations at a low computational cost, which aids in describing both flooding mechanisms' interactions during a compound flood event. Random sampling was used to create numerous combinations of these flooding mechanisms to develop the relative probability of compound flood levels.

To test this compound inundation model, a 1-D transect representing idealized low-gradient coastal watersheds was applied under various forcing conditions that vary in magnitude, time, and space. The compound flood hazard zones were based on the flooding mechanisms that dominated the region during the inundation and was divided into hydrologic, coastal, and transition flood hazard zone. The selected domain and 1-D approach allows for a more comprehensive analysis (rather than a 2-D model tested at a specific region) of the physical interaction of these flooding mechanisms from its most fundamental concepts, thus enhancing the definition of compound flood hazard zones for future flood hazard studies. The results deepen our understanding of the physical processes of compound flooding and inform future numerical model advancements.

2 Methods

2.1 Governing Equations

The two governing equations for the vast majority of the inundation models are the continuity and the momentum equations. These equations for gradually varied unsteady flow are often referred to as the St. Venant equations or the shallow water equations (Singh, 1996). The St. Venant equations are derived from the Navier-Stokes equations using various assumptions. These assumptions are well-summarized in Fiedler & Ramirez (2000) and Moussa & Bocquillon (1996). The one-dimensional (1-D) St. Venant equations are given as follows:

$$\frac{\partial H}{\partial t} + \frac{\partial UH}{\partial x} = 0 \tag{1}$$

$$\frac{\partial U}{\partial t} + U\frac{\partial U}{\partial x} + g\frac{\partial H}{\partial x} + F = 0 \tag{2}$$

where H represents the total water depth, U represents the depth-averaged water velocity, F is the friction forces, x represents the horizontal dimension, t represents the time, and g represents the gravitational acceleration force. The first term on the left-hand side of the momentum equation, Eq (2), represents the local acceleration, the second term represents the advective acceleration, the third term represents the pressure gradient, and the fourth term represents the frictional forces.

Depending on the domain being modeled (e.g., ocean or land), different terminologies for the governing equations are used. For example, rainfall runoff-driven inundation models choose the St. Venant terminology, while storm surge-driven inundation models select the shallow water terminology. This terminology also dictates how the friction force term in the momentum equation is handled. In the St. Venant terminology, the friction term is a function of the difference between the friction slope and the bottom slope (Moussa & Bocquillon, 1996). In contrast, in shallow water terminology, friction is formulated upon the bottom stress (Dietrich et al., 2005).

2.2 Numerical Model

Three separate algorithms were developed for the 1-D compound inundation model: i) a 1-D storm surge-driven inundation algorithm referred to herein as Coastal Hydraulics Module (CHM), ii) a 1-D rainfall runoff-driven inundation algorithm referred to herein as Watershed Hydraulics Module (WHM), and iii) a 1-D rainfall-runoff inundation algorithm referred to herein as Overland Hydraulics Module (OHM).

2.2.1 Coastal Hydraulics Module (CHM)

The two governing equations used in CHM are the 1-D primitive depth-integrated continuity equation and the 1-D primitive depth-integrated conservation of momentum equation in conservative form using shallow water terminology. The Generalized Wave-Continuity Equation (GWCE) (Eq. 3) was used in conjunction with the momentum equation's non-conservative form to improve the numerical solution's stability (Eq. 4,) (Dresback et al., 2004; Dresback & Kolar, 2001; Kinnmark, 1986). For simplicity, the following terms were not included: momentum dispersion, depth-integrated baroclinic forcing, equilibrium tide potential, depth-integrated horizontal momentum diffusion, atmospheric pressure, Coriolis force, and wind stress applied at the water surface (Luettich et al., 1992).

The 1-D CHM governing equations are represented as:

$$\frac{\partial^2 \eta}{\partial t^2} + G\frac{\partial \eta}{\partial t} + \frac{\partial}{\partial x}\left(U\frac{\partial \eta}{\partial t}\right) - \frac{\partial}{\partial x}\left(UH\frac{\partial U}{\partial x}\right) - g\frac{\partial}{\partial x}\left(H\frac{\partial \eta}{\partial x}\right) + (G-\tau)\frac{\partial UH}{\partial x} = 0 \tag{3}$$

$$\frac{\partial U}{\partial t} + U\frac{\partial U}{\partial x} + g\frac{\partial \eta}{\partial x} + \tau U = 0 \tag{4}$$

where η=H-h represents the free surface deviation, h represents the bottom depth, $\tau = C_f\, U/H$ represents the bottom friction, $C_f = n^2 g/H^{1/3}$ represents the friction coefficient, where n is Manning's friction coefficient, and G is the weighting parameter. The G parameter controls the relative weight of the primitive continuity equation, such that if $G \rightarrow \infty$, the equation becomes a pure primitive continuity equation, whereas if $G \rightarrow 0$, the equation becomes a pure wave continuity equation (Dresback et al., 2005).

Two boundary conditions were required to solve the system: i) water level time series imposed at the open ocean boundary, and ii) a zero-flow boundary condition imposed at the first

dry node. This water level time series represents the coastal forcings from the astronomic tides and storm surge flooding mechanisms in the open ocean. The first dry node is the subsequent node after the seawater front, where the seawater front is the farthest wet node from the open ocean boundary. Therefore, the CHM was applied from the open ocean boundary to the seawater front.

The solution of the system can be separated into three steps. First, the GWCE (Eq. 3) was solved for the free water surface deviation of the geoid at the future time step. This equation is dependent on the free surface water deviation at the current and previous time step and on the depth-averaged horizontal velocity at the current and previous time step. Second, a wetting and drying algorithm (WDA) updates the computational nodes' wet/dry status in the future time step (more details are provided in Section 2.4 and Text S1). Third, the momentum equation (Eq. 4) was solved for the depth-averaged velocity at the future time step. This equation is dependent on the free surface water deviation at the current and previous time step and on the depth-averaged velocity at the current and previous time step. Finally, these three steps were repeated for all the computational time steps until the total simulation time was reached.

2.2.2 Watershed Hydraulics Module (WHM)

The governing equations for the WHM are the continuity (Eq. 5) and momentum (Eq. 6) equations using the St. Venant terminology (Costabile et al., 2013):

$$\frac{\partial H}{\partial t} + H\frac{\partial U}{\partial x} + U\frac{\partial H}{\partial x} = r \tag{5}$$

$$\frac{\partial U}{\partial t} + U\frac{\partial U}{\partial x} + g\frac{\partial H}{\partial x} + g\left(S_f - S_o\right) = r\frac{U}{H} \tag{6}$$

where r represents the rainfall intensity, S_f represents the friction slope, and S_o represents the bottom slope. The St. Venant equations' simplified form, called the Kinematic Wave equations, provides an appropriate representation of the physics for shallow overland rainfall-runoff, especially in one dimension (Reddy et al., 2007; Singh, 2002; West et al., 2017). The idealized transect selected represents a coastal watershed floodplain where water can flow unconfined over the surface and not through a channel / river system, but since the model is 1-D, water can only flow in a single direction. Thus, the WHM only considers surface runoff, not flow through a channel / river. However, if desired, the WHM can simulate the riverine flow mechanism if the formulation is modified by changing the flow area and wetted perimeter from an overland terrain (e.g., bottom width is much greater than depth) to a confined channel. The Kinematic Wave equations neglect the local acceleration term, the convective acceleration term, and the momentum equation's pressure term (Eq. 6) (Moussa & Bocquillon, 1996). The source term in the momentum equation can also be neglected since it is an order of magnitude less than the other terms (Kazezyilmaz-Alhan et al., 2005). Therefore, the continuity equation (Eq. 5) reduces to a single dependent variable, *H*:

$$\frac{\partial H}{\partial t} + \frac{1}{n}\sqrt{S_o}\frac{\partial H^{5/3}}{\partial x} = r \tag{7}$$

The system's solution consists of solving the water depth in the continuity equation (Eq. 7) iteratively because of the system's non-linearity. Therefore, the Newton-Rapshon method was selected as the iterative solver technique (Santiago-Collazo & Silva-Araya, 2019). This technique consists of solving the system iteratively, at each time step, until the difference between two successive iterations is less than a specified tolerance (e.g., 10^{-7} m). Then, after convergence, the time step is incremented, and the iterative procedure is repeated. A WDA was employed after the new water depth solution had been computed. The WHM was applied only at the portion of the domain where the rainfall was falling. The WHM requires only one boundary condition to obtain a unique solution to the system, which is a zero-flow boundary condition and starts from a dry bed condition, meaning that all the nodes within the watershed region are considered to be dry at the initial simulation time.

2.2.3 Overland Hydraulics Module (OHM)

The OHM was developed to route the rainfall-runoff downstream through the portion of the domain where rainfall is not falling and the initial conditions are dry. This algorithm is identical to the CHM, except for the WDA's minimum water depth threshold and the boundary conditions. A flow boundary condition is the only boundary condition imposed on the OHM. This flow boundary condition represents freshwater from the rainfall-runoff computed by the WHM, recreating the downslope propagation of a flood wave over dry land. Therefore, water will travel freely until it reaches the seawater and gets coupled with the CHM. A similar approach could be to eliminate the OHM and use the CHM to simulate rainfall-runoff downstream of the domain. While this approach could potentially be more computationally efficient than the selected approach, the former will require a substantial improvement of the WDA, which is out of the scope of this study.

2.2.4 Coupling Technique

The following procedure outlines the compound inundation algorithm (see also Figure S1 for a graphical description):

1. The WHM was executed independently in the domain were rainfall was falling, and upon completion, the water depth and velocity time series at each node were stored.
2. The freshwater discharge time series at the outlet of the domain (computed in Step 1) was fed as a flow boundary condition in the OHM.
3. Compute the water surface deviation and depth-averaged velocity for the freshwater (computed by OHM) and seawater (computed by CHM) conditions simultaneously at each time step.
4. Step 3 was repeated for each time step until the following conditions were met: i) both the seawater and freshwater fronts were at the same node (i.e., coupling node), and ii) at least one of the water depths was greater than the minimum water depth threshold for the WDA of the CHM. If both conditions were met, then:
    a. The freshwater discharge was fed as a flow boundary condition to the CHM at the coupling node.
    b. The freshwater conditions (i.e., depth and velocity) upstream of the coupling node at the current time step were given to the CHM as the current conditions flooded by rainfall-runoff.

5. Compute the water surface deviation and depth-averaged velocity for the combined (i.e., freshwater plus seawater) conditions using the CHM at each time step until it reaches the total simulation time.
    a. If the combined waterfront is located within the WHM domain, the WHM freshwater discharge was fed as a flow boundary condition to the CHM at this location, similar to Step 2.
    b. If rainfall was still falling at the WHM domain after Step 4, the remaining rainfall was added to the CHM directly and not through OHM or WHM.
        i. The rainfall intensity term in the continuity equation of the WHM (Eq. 5) was added as a source term in the GWCE (Eq. 3) and multiplied by the weighting parameter (G).

2.2.5 Numerical Approach

A finite element discretization in space, such as the symmetrical weak weighted residual form, and finite difference discretization in time was used for each module. Regarding the finite difference discretization in time, a variably weighted, three-time-level, implicit scheme was applied for all the linear terms, while the non-linear terms were treated explicitly for the continuity equation of the CHM and OHM (Luettich et al., 1992). However, for the momentum equation, a two-time-level, implicit Crank-Nicolson approximation was applied to all terms except for the advective term, which is treated explicitly. Additionally, the Crank-Nicolson approximation was used for the time discretization of the continuity equation in the WHM and the rainfall intensity term in the GWCE.

The WDA plays a crucial role in any flood inundation model. The WDA is responsible for determining which elements will be included in the system's solution at each time step, depending on if they hold water. Also, WDA has been historically responsible for accurately capturing and describing the physics of the inundation / recession process that involves a flood wave propagating over dry land (Medeiros & Hagen, 2012). The WDA employed in all three modules were adapted from Dietrich et al. (2005) and Luettich & Westerink (1995a, 1995b). Further information on the WDA can be found in the supplemental text S1 and Dietrich et al. (2005).

2.2.6 Model Verification

Two different approaches are used to verify the 1-D compound inundation model. First, verification of the CHM and WHM was conducted against an analytical solution for each flooding mechanism. Second, a mass balance analysis was performed to verify the coupled WHM-OHM system and the compound inundation model since no analytical solution can describe the compound flood dynamics. Validation for this type of 1-D model requires laboratory measurements (beyond the scope of the study) or observed data during a compound flood event, which is not feasible since a 2-D model is required to account for all possible interactions, especially at low-gradient coastal land-margins. Therefore, the verification approach selected is considered pertinent due to the circumstances mentioned above.

2.2.6.1 Analytical Solution

The CHM was verified against an analytical solution of a "frictionless" beach presented by Carrier and Greenspan (1958). This analytical solution describes the behavior of a frictionless

wave on a linearly sloped beach. The shoreline was computed for this linearly sloped beach using the CHM (Figure 1a). During the first 12 hr of the simulation (i.e., the first tidal cycle), the CHM experiences some start-up noise, which differs from the analytical solution. This behavior occurs because the CHM does not employ a ramp function at the start of the simulation to smooth the transition from a cold start. After the first tidal cycle, there is a good agreement in the shoreline position computed by the CHM and the analytical solution, especially during the tides' flood (i.e., shoreline position at 21 km). However, there is a slight difference of ~100 m between both solutions of the shoreline position when the tides are ebbing (i.e., shoreline position at 18.8 km). This difference is because the analytical solution was formulated assuming frictionless conditions (i.e., $C_f = 0$) of the surface, but the CHM formulation does not allow a bottom friction coefficient of zero; therefore, a relatively small value (i.e., $C_f = 0.001$) had to be assigned. This relatively small bottom friction coefficient does not dominate the momentum balance. Therefore, no friction-induced lag was shown between both solutions of the shoreline position. Similar findings were presented by Dietrich et al. (2004).

The WHM was verified against an analytical solution of a hypothetical watershed by Gottardi and Venutelli (1993). This analytical solution represents a rainfall-runoff routing produced by a constant rainfall in space and time through a linearly sloping uniform terrain (i.e., paved parking lot). The rainfall-runoff hydrograph at the watershed outlet was computed using the WHM and the analytical solution (Figure 1b). The rainfall-runoff increases for both solutions until the time of concentration, which represents the watershed's total contribution to the rainfall-runoff at the outlet (i.e., rainfall-runoff travel time from the hydraulically most distant point in the watershed to the outlet). For this hypothetical watershed, the time of concentration was 73 min. The rainfall-runoff hydrograph remains constant after exceeding the time of concentration and while rainfall is still falling over the watershed. This behavior represents that the watershed has reached its maximum flow capacity, which for this hypothetical case is 7.9 m^3 hr^{-1} m^{-1}. After the rainfall ends, the rainfall-runoff decreases until the watershed is drained. Overall, there is a good agreement between the rainfall-runoff computed by the WHM and the analytical solution at this hypothetical watershed outlet. Similar findings were presented by Reddy et al. (2007). A full description of both case studies, including parameters and domain description, can be found in the supplemental text S2.

2.2.6.2 Mass Balance Analysis

Any shallow water model must be verified for conservation of mass, especially a continuous Galerkin finite-element model (Dietrich et al., 2008), such as the one presented in this study. The Finite Volume method (Kolar et al., 1994) was used to compute the global mass residual and is presented in the supporting information text S3. A global mass balance analysis was performed to evaluate the coupled WHM-OHM system and the compound inundation model due to the lack of an analytical solution. The environmental forcing selected for this analysis was a tidal amplitude of 10 cm, a peak storm surge of 97 cm, and a rainfall accumulation of 248 mm during an entire day. The total simulation time was 40 days, in which rainfall fell at the upper segment of the transect during the 2nd day, and the peak storm surge occurred during mid-day of the 4th day. The global mass balance error for the routing of rainfall-runoff using the coupled WHM-OHM system was 1.0 kg m^{-1}. For the compound inundation model, the global mass balance error was 33.6 kg m^{-1}.

As a basis for comparing the mass balance analysis results presented above, the mass balance analysis done by Dietrich et al. (2005) was recreated using the simulation results from the CHM. The environmental forcing selected for this analysis was only a tidal amplitude of 1.0 m with a tidal period of 12 hr. The modeling domain consisted of a three-segment transect with a horizontal middle segment at a 0.5 m elevation. The net flux and accumulation terms for the global mass balance analysis at the middle segment were computed using CHM (Figure 2c). There is a good agreement between the net flux and accumulation terms, meaning that the mass balance residual is low throughout the simulation. The positive values represent that mass is entering the control volume (i.e., middle segment), while the negative values represent that mass is leaving. This behavior coincides with the ebbing and flooding of the tides. Overall, the global mass balance error was 123 kg m^{-1} using the CHM, representing 6.4% of the average net flux or accumulation terms. In comparison, Dietrich et al. (2005) reported 5,662,000 kg m^{-1} as the best global mass balance error estimate for a 2-D domain (i.e., x- and z-axis) that consisted of 11 vertical layers, which approximates 515,000 kg m^{-1} per vertical layer. Therefore, this result represents that the compound inundation model and the coupled WHM-OHM system conserve mass relatively well compared to previous studies.

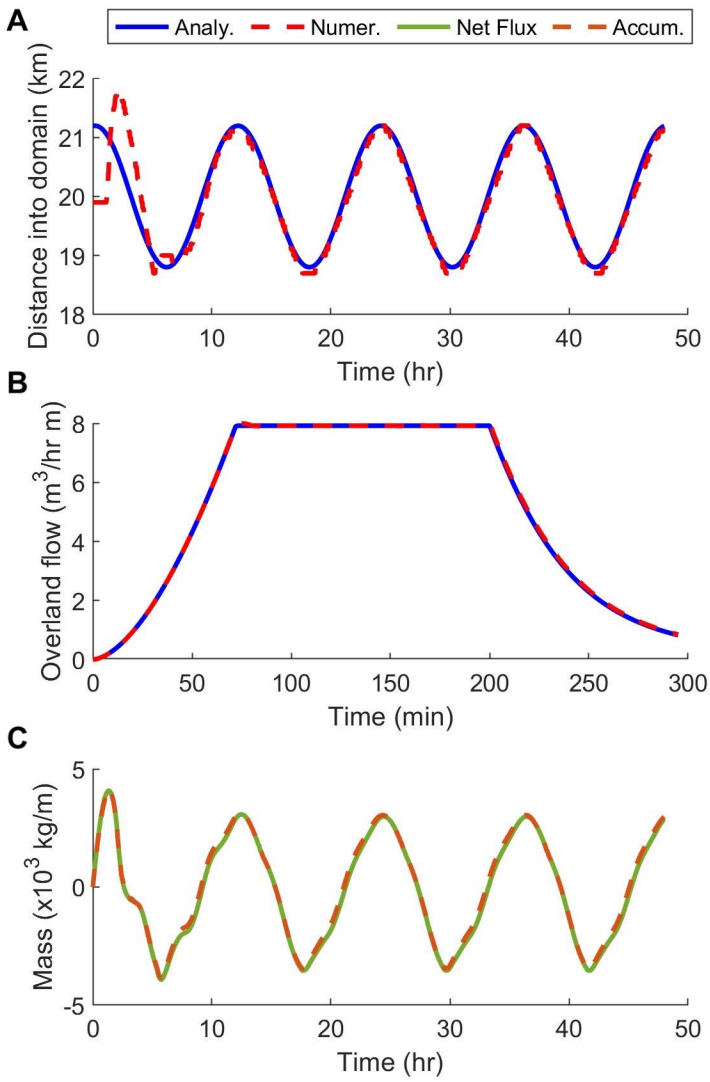

Figure 1. Numerical model verification based on an analytical solution (a-b) and a mass balance analysis (c). The (a) Coastal Hydraulics Module and (b) the Watershed Hydraulics Module were tested against an analytical solution, while the a (c) mass balance analysis was performed at the domain's middle segment using the Coastal Hydraulics Module. The solid blue line represents the analytical solution computations, while the red dashed line represents the individual numerical module computations. The solid green line represents the net flux term, while the dashed black line represents the accumulation term (created using MATLAB).

2.3 Model Configuration

2.3.1 Model Domain: Idealized Coastal Watershed Transect

This study uses an idealized transect to represent a "simplified" description of a low-gradient coastal watershed. Thus, eliminating many complexities from the flood response due to microtopography, small channels, and surface roughness variations. The generated idealized transect was 123 km in length and divided into three segments: lower, middle, and upper (2). The

lower segment has a length of 40 km from the beginning of the domain and a slope of 0.5 m km^{-1}. The middle segment extends from 40 to 78 km with the mildest slope in the domain (e.g., 0.005 m km^{-1}), while the upper segment covers from 78 to 123 km with a steeper slope of 0.1 m km^{-1}. These values represent the typical landscape within the Sabine and Mermentau River Watersheds (See location in Figure S2). Additional details on the development of this idealized transect can be found in supplemental information text S4.

The domain was described in terms of flow resistance by assigning a constant surface roughness coefficient for each segment. Manning's friction coefficients of 0.02, 0.03, and 0.04 were assigned to the lower, middle, and upper segments, respectively. For example, Manning's friction coefficient for the lower segment represents open water since this segment is completely submerged under mean sea-level conditions (Mattocks & Forbes, 2008). However, the selected value for the middle segment represents the average conditions encountered in the observed transects, such as open water and emergent estuarine wetland, while for the upper segment was an average of shrubs, scrubs, and cultivated land.

For this study, rainfall fell only at the upper segment of the generated idealized transect. Thus, the OHM was only applied to the middle segment. The CHM boundary conditions were specified at the open ocean boundary (i.e., 0 km into the domain), while the OHM boundary conditions were at the middle segment's upstream end. The zero-flow boundary condition of the WHM was applied at the most upstream node of the upper segment.

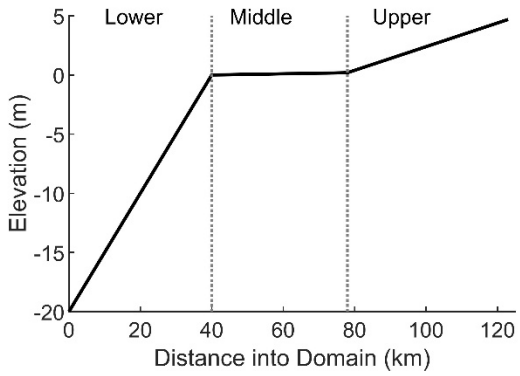

Figure 2. Generated one-dimensional idealized coastal watershed transect. Notice that the transect is vertically exaggerated to show the profile details (the x-axis is in kilometers, and the y-axis is in meters). (created using MATLAB)

2.3.2 Environmental Forcings

Three flooding mechanisms (rainfall-runoff, storm surge, and astronomical tides) were simulated. To create a compound flood event, variations of antecedent rainfall and tropical cyclone (including tides) events were created. The antecedent rainfall inundates the domain by pouring a uniform rainfall intensity over the upper segment, which flows downstream towards the middle segment in the watershed outlet's direction (i.e., 40km into the domain). This rainfall event resembles the intense and prolonged rainfall brought upon by low-pressure systems or warm fronts that bring moisture from the Gulf of Mexico into the mainland. Rainfall frequency maps from the NOAA's Atlas 14 were used to characterize the rainfall intensity from the antecedent rainfall event (Bonnin et al., 2006). To have an overall representation of the coastal

Louisiana rainfall estimates, the quantile estimates for all the rain gauges (~ 30) bounded south of I-10 and US-90 (see Figure S4 for location) were averaged into a single dataset of rainfall intensity for the 2- to 100-yr return periods and rainfall durations between one to three days (see Table 1). The Atlas 14 dataset was selected due to its capability of having quantile estimates for rainfall events lasting more than 24 hr. However, the authors recognize that other parametric methods, such as those developed by the Southeast Regional Climate Center (Faiers et al., 1997; Keim & Faiers, 2000) fit the observed data in coastal Louisiana more accurately than the ones from the Atlas 14, but are limited to 24-hr rainfall events.

Table 1. Quantile estimates for the average rainfall conditions in coastal Louisiana based on the Atlas 14 dataset.

Return Period (yr)	Rainfall Duration (hr)					
	Rainfall depth (mm)			Rainfall intensity (mm hr^{-1})		
	24-hr	48-hr	72-hr	24-hr	48-hr	72-hr
2	128	147	159	5.34	3.07	2.21
5	170	197	212	7.09	4.10	2.95
10	207	240	258	8.64	4.99	3.58
25	264	304	326	10.98	6.33	4.53
50	312	358	384	12.98	7.46	5.33
100	364	416	446	15.17	8.67	6.19

A tropical cyclone event will follow the antecedent rainfall event, whereby these two events are mutually exclusive. The flood elevations given by the Flood Emergency Management Agency (FEMA) flood insurance study of Louisiana's Southeastern parishes (FEMA & USACE, 2008) were used to characterize the storm surge flooding mechanisms from the tropical cyclone event. For example, the flood elevations at -20 m NAVD88 in coastal Louisiana range from a maximum of 0.97 to 1.73 m for the 10- and 100-yr return periods, respectively. These flood elevations were considered the direct contribution of the storm surge flooding mechanisms. An empirical equation (Xu & Huang, 2014) for developing storm surge hydrographs were used to recreate the storm surge conditions at the open ocean boundary.

$$H_t = \begin{cases} H_p\left(1 - a \times e^{-|b/t - t_0|}\right) \\ H_p\left(1 - c \times e^{-|d/t - t_0|}\right) \end{cases} \quad (8)$$

where H_t represents the water height time series due to the storm surge, H_p represents the peak storm surge at landfall time, t is the time within the time series, t_0 represents the time at landfall, and a and b represent the fitted parameters for the rising limb, while e and d for the falling limb. This equation is based on observed storm surge hydrographs induced by category 3 and 4 hurricanes at several coastal stations within the US Gulf of Mexico. For this study, the storm surge hydrograph produced by a category 3 hurricane was used. Any rainfall associated with the tropical cyclone event was neglected since the selected forcing does not provide any tropical cyclones characteristics, such as radius, winds speed, forward motion, and central pressure. These characteristics are essential in most parametric rainfall models, such as the IPET model (see Bislkie et al., 2021), to estimate the spatial- and temporal-varying tropical cyclone-driven rainfall. Thus, the simulated meteorological event is similar to a strong and persistent onshore wind event, producing storm surge flooding without any rainfall associated with the system.

The flooding and ebbing of the astronomical tides were considered throughout the compound flood event's entire duration. As the astronomical tides flood, seawater inundates the middle segment, and as the tides recede, seawater retreats and moves toward the lower segment. A constant-amplitude, single-frequency tidal signal was used to represent the tidal flooding within the modeling framework. This tidal signal was applied at the open ocean boundary using a sinusoidal function. Therefore, the tidal signal was superimposed on the storm surge hydrograph to obtain the open ocean boundary's total water level.

A tidal resynthesis analysis of observed data (NOAA, 2021) was performed to determine the tidal amplitude for coastal Louisiana during a 14.7-day tidal cycle. The daily tidal amplitude was computed as one-half of the mean daily tide range from the tidal resynthesis analysis performed at each of the ten NOAA stations selected (see Figure S4 for location). The spring tide amplitude was selected as the representative tidal amplitude for the compound flood event since it is the highest tidal water level. The spring tide amplitude averaged throughout coastal Louisiana was 0.43 m and represented the Gulf of Mexico's microtidal range. Similarly, the diurnal tide behavior selected mimics the conditions in the Gulf of Mexico.

The compound flood event timing was varied to determine the total water level response due to the multiple forcings and their relative timings. The flood event timing is defined as the time between the end of the antecedent rainfall event and the arrival of the peak storm surge. For example, suppose the antecedent rainfall event finishes at the end of the second day of the simulation. In that case, the tropical cyclone effects can arrive as early as the third day to as late as the fifth day of the simulation (0 – 48 hrs). The start of the antecedent rainfall event will not vary within the compound flood event timeline since, by definition, it occurs before the storm surge arrives. The duration of the antecedent rainfall event varies from 24 to 72 hr, since previous studies have found antecedent rainfall events up to 3 days before a tropical cyclone landfall in this region (Bilskie et al., 2021).

2.3.3 Model Setup

The 1-D compound inundation model was specified to run a 7-day simulation with a computation time step of 10 seconds. The element size was 200 m, totaling 616 computational nodes for the selected idealized transect. The combination of this time step and element size results in a Courant-Friedrichs-Lewy (CFL) condition of 0.7, which is within the recommended range to avoid numerical instabilities (Mahgerefteh et al., 2009). The weighting parameter G was set to 0.03 throughout the entire domain (Westerink et al., 2008) since the maximum bathymetric depth (-20 m) is relatively shallow when compared to the deepest portion of the Gulf of Mexico (~ 5 km). A different minimum water depth threshold (H_o) and minimum velocity threshold (U_{min}) were used for each module. For the WHM, H_o and U_{min} were established as 10^{-3} mm (Brufau et al., 2004) and 10^{-3} mm s^{-1}, respectively. For the CHM, H_o and U_{min} were set as 50 mm (Bilskie et al., 2021) and 50 mm s^{-1}, respectively. Finally, the H_o and U_{min} selected for the OHM were 1 mm (R.A. Luettich & Westerink, 1995b) and 1 mm s^{-1}, respectively.

2.4 Simulation Set

A random sampling technique (RST) was used to select the simulation set and assess the total water level's behavior under multiple combinations of the flooding mechanisms. The rainfall-runoff and storm surge mechanisms varied in magnitude and timing for the RST. For example, the rainfall intensity, duration of the rainfall event, peak storm surge level, and peak

storm surge time were selected as part of the RST. These parameters were varied between their upper and lower bounds, specified in Section 2.3.2, and were combined based on an equal probability of occurrence. A more "realistic" probabilistic distribution, rather than uniform distribution, was not pursued since the statistical behavior of the flooding mechanisms was out of scope for this study. However, the authors recognize the complex probabilistic distribution a compound flood event could entail, and thus are aware that certain combinations generated using the RST approach might be unrealistic but are suitable for this initial study.

The rainfall intensity was set to vary between the 2- and 100-yr return periods (See Table 1), with the rainfall duration set to vary between 24 to 72 hours. To estimate the exact quantile estimate, a power curve was fitted to the values on Table 1 based on the different return periods. In other words, six curves (See Figure S5), with their respective equations, are used by an algorithm to interpolate the exact value using a bilinear interpolation technique. For example, if the RST selects a rainfall event with a 36.8-yr return period magnitude lasting 67.48 hr, the fitted curves will be used to compute the quantile estimate at both bounds of the magnitude (25- and 50-yr) and duration (48 and 72 hr), and then interpolate the exact value (4.97 mm hr^{-1}). The peak storm surge level at the open ocean boundary varied between the 10- and 100-yr return periods with a time to peak between 0 and 48 hr after the rainfall event ended. 1,000 different combinations of these four input parameters were produced as part of the RST. A subset of eight different combinations is shown in more detail in the supporting text S5 and Table S1.

The combination of the selected idealized transect and the diurnal micro-tides selected for this study requires that all simulations start from a hot start rather than from a cold start. This hot-start represents the sea-level conditions at dynamic equilibrium with the tidal forcing only and is required due to the model's absence of a ramp function. Therefore, to avoid additional simulations required to produce the hot start conditions for each of the RST combinations, a single hot start condition was selected for the completed set of combinations. This selected hot start condition represents a 60 days simulation with spring tide at the selected idealized transect.

Three different flooding scenarios were evaluated using each of the RST combinations. These flooding scenarios are i) storm surge only, ii) antecedent rainfall event only, and iii) the combined storm surge and antecedent rainfall events. All three flooding scenarios include the astronomical tides flooding mechanism throughout the entire simulation period. These flooding scenarios resulted in three simulations for each RST combination, with 938 combinations per scenario evaluated. Note that approximately 6% of the combinations (i.e., 62 out of 1,000) where eliminated from the simulation set since these combinations had a rainfall intensity less than the 2-yr event. Therefore, 2,814 simulations were performed to assess the compound flood at the selected idealized transect.

2.5 Post-Processing Techniques

2.5.1 Flood Hazard Zones Delineation

Compound flood hazard zones (FHZs) can be delineated based on the flooding mechanism that dominates the total water levels at a particular region. Thus, three FHZs can be delineated: coastal, hydrologic, and transition (Bilskie & Hagen, 2018). Three separate flooding scenarios have to be simulated to delineate the flood hazard zones. The flooding scenarios considered are rainfall-runoff and tides, storm surge and tides, and the combination of rainfall-runoff, storm surge, and tides. Researchers have recently used two techniques to delineate the

565 FHZ based on the different flooding scenarios. Bilskie and Hagen (2018) defined the transition
566 zone where the maximum water levels from the rainfall-runoff scenario are greater than the
567 water levels from the storm tides scenario, and the water levels from the combined scenario are
568 greater than the water levels from the rainfall-runoff scenario (Bilskie et al., 2021; Bilskie &
569 Hagen, 2018). Similarly, the technique used by Shen et al. (2019) consists of defining the
570 transition zone as areas where the combined scenario elevations are at least higher than the
571 simulation of either flooding mechanisms by a specific threshold, such as 10 – 20 cm (Gori et al.,
572 2020b; Shen et al., 2019).

573 This study defined the compound FHZ using the maximum water level from three
574 individual flooding scenarios: rainfall-runoff only (R), storm surge only (S), and the combined
575 (RS) scenario. The coastal FHZ is defined as the region where the maximum water level from
576 the storm surge scenario is approximately equal (< 10 cm) to the water levels from the combined
577 scenario ($\eta_S \cong \eta_{RS}$). The hydrologic FHZ was defined as the region where the maximum water
578 level from the rainfall-runoff scenario is approximately equal (< 10 cm) to the water levels from
579 the combined scenario ($\eta_R \cong \eta_{RS}$). Finally, the transition FHZ was defined as the region where
580 the maximum water levels from the combined scenario were greater than the water levels from
581 the storm surge and rainfall-runoff scenarios ($\eta_S < \eta_{RS}$ and $\eta_R < \eta_{RS}$).

582 2.5.2 Flood Rank

583 A flood rank (F_R) (Eq. 9) was developed to interrogate the diverse response of the total
584 water levels due to the variations in environmental forcings. This ranking compares the
585 maximum water levels from a given simulation with the maximum of maximums and minimum
586 of minimums of water levels of the combined flood scenario. Therefore, each simulation will
587 have a F_R at each computational node, with values ranging from 0 to 1. As $F_R \rightarrow 0$, the
588 maximum water levels for a given simulation are closer to the minimum of minimums, meaning
589 that the simulation has the least severe inundation. Conversely, as $F_R \rightarrow 1$, the maximum water
590 levels for a given simulation are closer to the maximum of maximums, meaning that the
591 simulation has the most severe inundation. Since F_R varies spatially within each simulation, the
592 average F_R (i.e., $\overline{F_R}$) can be computed at different regions of interest within the domain, such as
593 compound flood hazard zones or changes in slope. $\overline{F_R}$ represents what *really* happened in terms
594 of the inundation levels, given a set of environmental forces:

$$\overline{F_R}_j = \frac{1}{N}\sum_{i=1}^{N}\frac{\eta^i{}_j - \eta^i{}_L}{\eta^i{}_u - \eta^i{}_L} \quad (9)$$

595 where the superscript i represents the node index, N represents the total amount of nodes within
596 a region, the subscript j represents the simulation ID, the subscript u represents the maximum
597 water level from the entire simulation set at node i, and the subscript L represents the minimum
598 water level from the entire simulation set at node i.

599 2.5.3 Severity Index

600 The severity index (SI) serves as a tool for determining how a combination of forcing's
601 parameters could translate into inundation effects. The storm surge peak time (s_t) was
602 considered with respect to the high astronomic tide level (s_{tA}) and the end of the antecedent
603 rainfall event (s_{tR}). The "best" case (or less severe) was when all input parameters were at their

minimum value, such as r_m= 4.36 mm hr^{-1}, r_t= 24 hr, s_m= 0.97 m, and s_{tR}= 48 hr, and the storm surge peak time coincides with a low astronomic tide level, which occurs from 12 to 156 hrs every 24 hours. This represents a $SI = 0$. Conversely, the "worst" case (or more severe) is when all input parameters are at their maximum value, such as r_m= 6.19 mm hr^{-1}, r_t= 72 hr, s_m= 1.73 m, and s_{tR}= 0 hr, and the storm surge peak time coincides with a high astronomic tide level, which occurs from 6 to 150 hrs every 24 hours). This represents a $SI = 1$. Thus, the SI represents what *could* happen, in terms of the inundation levels, given a set of environmental forces, and was defined as:

$$S_j = (\theta_1 {r_t}^* + \theta_2 {r_m}^* + \theta_3 {s_m}^* + \theta_4 {s_{tA}}^* + \theta_5[1 - {s_{tR}}^*])_j \quad (10)$$

where θ represents an unknown weighting coefficient for each input parameter, r_t represents the rainfall duration, r_m represents the rainfall intensity, s_m represents the peak storm surge level, s_{tA} represents the peak storm surge time with respect to the high astronomical tide level, s_{tR} represents the peak storm surge time with respect to the end of the antecedent rainfall event, and the superscript * represents the normalized value of a given parameter. Note that the reciprocal of s_{tR} is considered in Eq.10 since it is assumed that a more severe index occurs when the time between the peak storm surge and the end of the antecedent rainfall events is at its minimum (e.g., 0 hr) and not as the maximum as the other parameters in this equation.

An ordinary least-squares regression (K. Haddad et al., 2011; Khaled Haddad et al., 2013) was used to find the weighting coefficients of SI within each region of interest for the complete simulation set. This technique optimizes the weighting coefficient values by minimizing the square difference between the F_R and the SI for the entire simulation set at each region of interest. In other words, a perfect correlation occurs when $F_R = 1$ and the $SI = 1$, meaning that the worst case of combinations of inputs parameters resulted in the highest flood levels. Two constraints were specified to determine these weighting coefficients. First, the sum of the weighting coefficients must equal one since the S (Eq. 10) represents a weighted average of the input parameters. Second, the values of the weighting coefficients must be between zero and one ($0 < \theta < 1$).

3 Limitations

Some of the model's limitations were based on removing some natural processes when developing the proposed modeling framework. For example, some of the omitted hydrologic processes were infiltration, percolation, evapotranspiration, interception, initial soil moisture, and initial abstraction. These neglected components, if considered, will decrease the overland rainfall-runoff that will eventually interact with the seawater and increase the compound inundation. However, for return period analyses such as those conducted herein, these could likely be included as uncertainty terms. Also, during extreme weather events, such as the ones simulated in this study, these neglected components often have a minor impact on the flood depths, especially when combined with the peak storm surge (Huang et al., 2021).

Similarly, some neglected coastal processes were momentum dispersion and diffusion, baroclinic forcing, atmospheric pressure, Coriolis force, and wind stress applied at the water surface. These omitted factors, in addition to the rainfall from the tropical cyclone, will influence the water level at the lower segment and subsequently alter the compound flood hazard zones.

While the hydrologic and coastal process limitations deserve further study, the latter will likely lead to more complicated non-linear interactions. However, the model formulation was developed to include such components in future studies easily. For example, the neglected coastal processes can be included based on the well-developed ADCIRC formulation (Luettich et al., 1992), on which this model is based. Similarly, hydrologic processes neglected can be included as source/sink terms in the continuity equation (Eq. 5) based on spatially varying watershed properties, such as LULC and soil types.

Lateral discharge was neglected in the modeling framework due to its 1-D nature, thus, limiting the validation capability of the proposed framework with other published studies of our models, which are mainly 2-D. However, the purpose of this tool was never to estimate or forecast the compound flood level, which requires 2-D models, but rather to assess the relationship between flooding mechanisms in a controlled environment. This would bring some knowledge when expanding this effort into 2-D. Another limitation of the selected modeling framework was the inclusion of riverine processes, such as river flow, out-of-bank flow, and depth-varying roughness. The selected framework considers only overland flow produced from rainfall-runoff. However, the governing equations of the WHM can be modified by changing the flow area and hydraulic radius parameters from a very wide channel option (overland flow) to a conveyed flow through a defined cross-section (riverine flow).

The authors acknowledge that the modeling framework's computational efficiency could be improved in future research. For example, the CHM can replace the OHM if the appropriate boundary conditions are applied. Also, this effort would require improving the current wetting and drying algorithm by lowering the current water depth threshold to propagate shallower flow. In addition, the current coupling technique employed between the hydraulic modules (i.e., one-way coupling) does not allow the continuous transfer of information between them. This means that coastal processes from the CHM do not affect the solution of the WHM. Recall that the Kinematic wave assumptions do not support backwater effects due to neglecting the pressure gradient term in the momentum equation (Eq. 6). Thus, the coastal process's backwater effect cannot be computed by the WHM. Future work should focus on applying more robust techniques, such as the diffusive wave assumption. Regardless of these limitations, this study's findings support the need for a more holistic assessment of compound inundation in low-gradient coastal watersheds, improving the compound FHZ's delineation.

4 Results

4.1 Time-varying Water Level and Velocity Profiles: Simulation #692

The proposed 1-D compound inundation model outputs were time- and space-varying water surface elevation and velocities. Post-processing these outputs can lead to the creation of water levels and flow profiles. For example, the water surface elevation (WSE) and flow profiles for Simulation #692 (See Table S1 for more detail) are presented in Figure 3 at different simulation times. Note that the ordinate of the WSE profiles (Figure 3A, C, E) was exaggerated (i.e., ordinate in meters vs. abscissa in kilometers) to enhance the water level variations along the idealized transect.

When the antecedent rainfall event ends, the WSE profiles of the R and RS scenarios overlap beyond 43 km into the domain (Figure 3a). Conversely, the WSE profiles of the S scenario overlap the RS scenario downstream of 70 km into the domain. However, the flow

687 profiles (Figure 3b) illustrate that there is no water movement between the 43 to 70 km of the
688 middle segment. This means the water levels over this region are ponded seawater from the tidal
689 spin-up. However, the tides are pushing seawater into the middle segment and propagating
690 upstream only 3km, while the rainfall-runoff is inundating the first 9 km of the upstream portion.
691 Therefore, both flooding mechanisms can affect the same region simultaneously without
692 exacerbating their individual flooding effects. As time progress, the freshwater will travel
693 downstream until it meets the seawater from the storm surge. For example, when the peak storm
694 surge arrives, it inundates the lower 13 km of the middle segment with seawater, while
695 freshwater flows seaward and floods more than half of the segment (Figure 3c). However, at this
696 time step, it can be seen that there has not yet been a flux interaction between the storm surge
697 and the rainfall-runoff since there is a dead flow zone between 53 and 56 km of the middle
698 segment (Figure 3d).

699 As the storm surge wave propagates inland, it dominates the inundation levels for more
700 than half of the segment (58 km into the domain) since the RS and S scenarios overlap in Figure
701 3e. However, there is evidence that both flooding mechanisms exacerbated their individual
702 inundation impacts since, for the RS scenario, the water level was higher than both individual
703 scenarios between 60 to 72 km of the middle segment. Also, the flux interaction between both
704 processes resulted in a slight ,0.05 $m^3 s^{-1} m^{-1}$, attenuation of the storm surge flooding effects since
705 the RS scenario has a lower flow than the S scenario inland (Figure 3f). For the remainder of the
706 simulation period (not shown here), the water levels from all the flooding scenarios will decrease
707 gradually since the only mechanism driving the flood is the astronomical tides. The compound
708 FHZs, as well as the location and time of the maximum inundation levels, can be obtained from
709 the outputs of this modeling framework under different flooding scenarios and will be discussed
710 in more detail next.

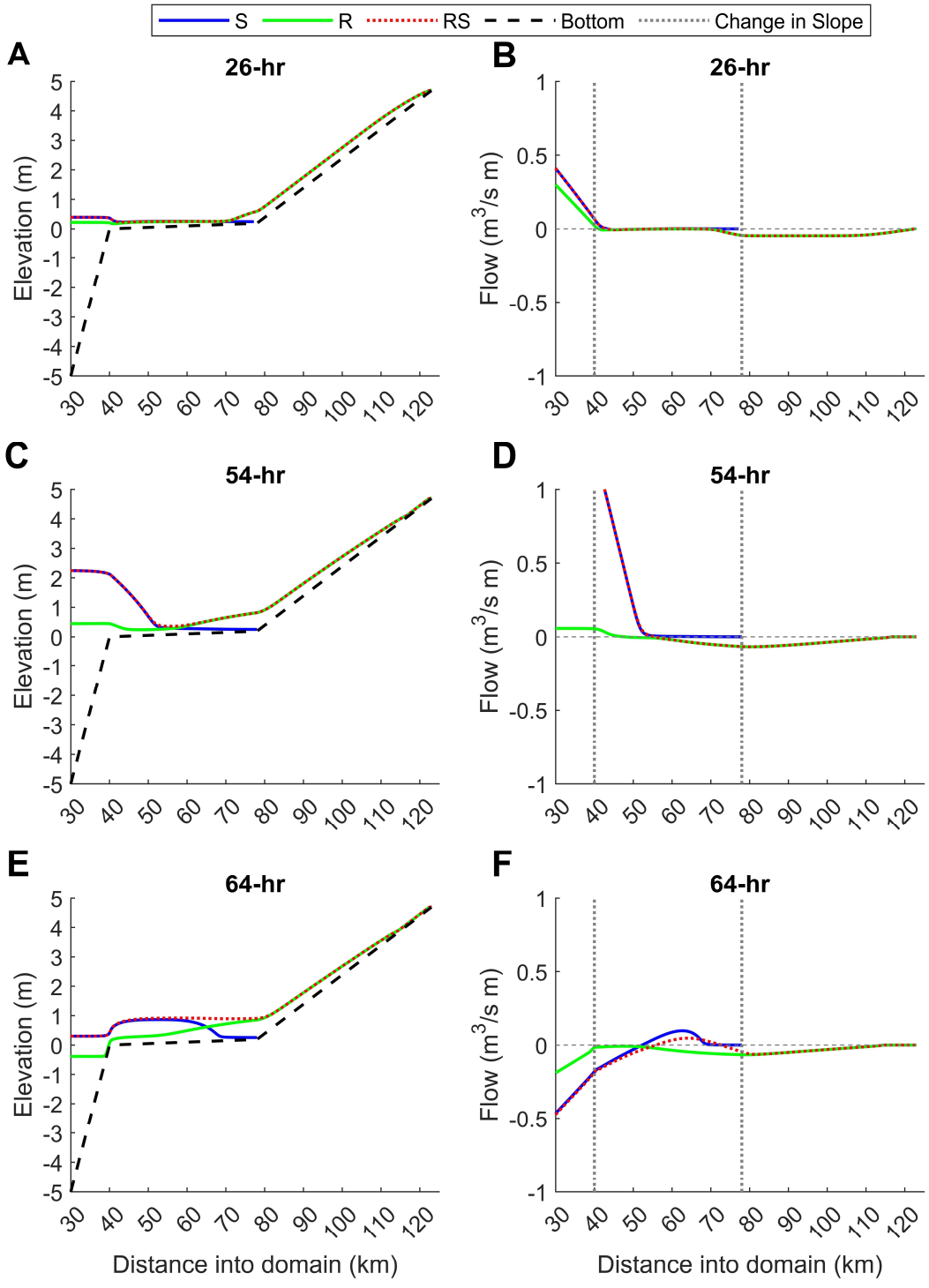

711

712 **Figure 3**. Water surface elevation and flow profiles at different times for Simulation #692 under
713 various flooding scenarios. The blue and green solid lines represent the storm surge only (S) and
714 rainfall-runoff only (R), respectively, while the red dotted line represents the combined flood
715 (RS) scenario. The dashed black line represents the bottom profile. The title of each subpanel

refers to the simulation time. The dashed grey line represents the zero-flow value. The grey dotted lines represent the change in the slope of the idealized transect. The title of each subpanel refers to the simulation time. Positive flow values represent that water is moving landward, while negative values represent that water is moving seaward (created using MATLAB)

4.2 Maximum Water Level

The maximum water level (MWL) and the time to peak water level (TPWL) profiles were computed for the simulation set under different flooding scenarios. The MWL profiles were obtained by selecting the MWL during each computational node's entire simulation period. The TPWL profiles were computed as the simulation time when the MWL occurred at each computational node. Notice that the linear superposition of the individual flooding scenarios profiles (R+S scenario) was computed by adding linearly the WL time series at each node from the S and R scenarios, followed by subtracting the WL time series of the tides only scenario at each node to remove the double accounting of tides from combining both scenarios. Then, the MWL at each node for the entire series was computed to obtain the MWL profiles for the R+S scenario.

WSL profiles (Figure 4) from the simulation's subset (Table S1) illustrate that the forcing's magnitude and timing affect the compound inundation levels. For example, the most critical combination in terms of magnitude, high rainfall and high surge, had the greatest inundation levels in the middle segment. However, the compound inundation levels were their lowest when the rainfall lasted longer. In addition, there was a greater separation between the end of the rainfall and the peak storm surge since you will have a less intense rain event with more time to drain before the storm surge event. Furthermore, the R+S profiles had a greater value than the RS scenario for all the simulations within the middle segment. Thus, illustrating the non-linearity between the flooding mechanisms in a compound flood at the "potential" transition zone.

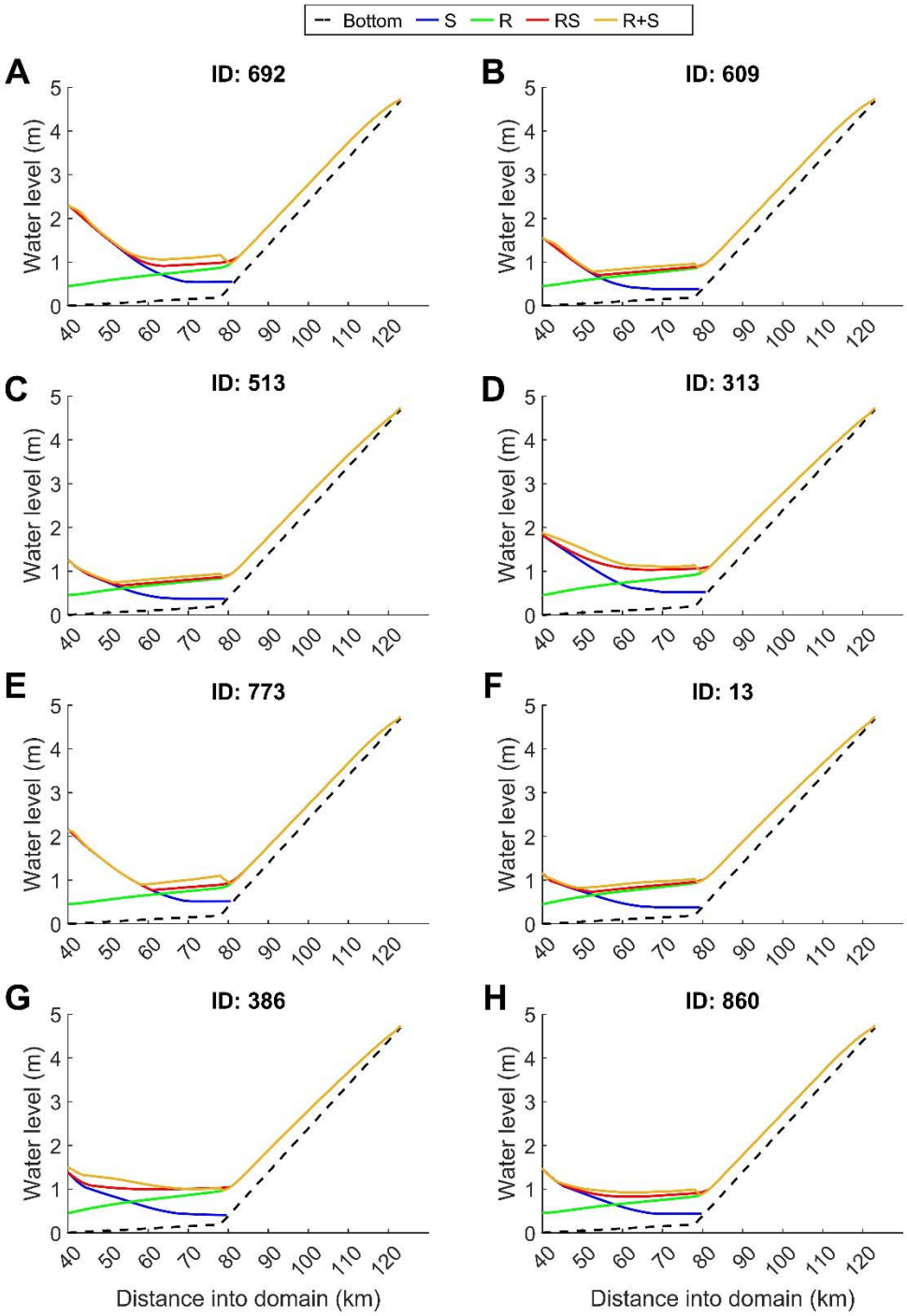

Figure 4. Maximum water level profiles for different flooding scenarios of the simulation subset (Table S1). The solid blue, green, and red lines represent the storm surge only (S), rainfall-runoff only (R), and combined flood (RS) scenarios, respectively. The solid yellow line represents the linear superposition of the water levels computed by the rainfall-runoff-only and storm surge-

only (R+S) scenarios. The dashed black line represents the bottom profile. The title of each subpanel refers to the simulation ID within the subset. (created using MATLAB)

In terms of TPWL profiles, the simulation's subset results (Figure 5) show the astronomic tides flooding mechanism segmenting the profiles due to seawater being pushed landward at each high tide within the tidal period (~ each 16 hr) and increasing its MWL. Note that this time does not coincide with the time between successive high and low tides (12 hours) since the storm surge hydrograph's falling limb influences the water levels. Therefore, the astronomical tides mechanisms can have an essential role in the TPWL profiles in all scenarios. Furthermore, a pseudo-linear behavior of the TPWL profile at the middle segment can be identified for the RS scenario. This can be attributed to the exchange of momentum between both flooding mechanisms since the seawater flow penetrating inland under the peak storm surge conditions can have enough momentum to push the freshwater flow landward and further increase the middle segment's growth total water levels. For certain flood hazard combinations, such as Simulation 773 and 13, the two flooding mechanisms may occur almost (within 2 hr) simultaneously but at different locations within the middle segment (Figure 5e-f). As time progressed, the flood waves would coincide, creating a compounding flood event, which could aggravate or alleviate the inundation levels. In certain simulations (773), the TPWLs for all three scenarios can occur at the exact location (78.8 km) within one hour (Figure 5e). However, water level hydrographs at this location illustrate that if the individual flooding mechanisms were linearly superposed, the total water levels overestimate the total inundation when the flooding mechanisms are not considered in a compound modeling framework (Figure S6). Therefore, the non-linearity of a compound inundation is not only because of the different time-to-peak water levels from each flooding mechanism, and additional factors should be considered, such as the momentum exchange.

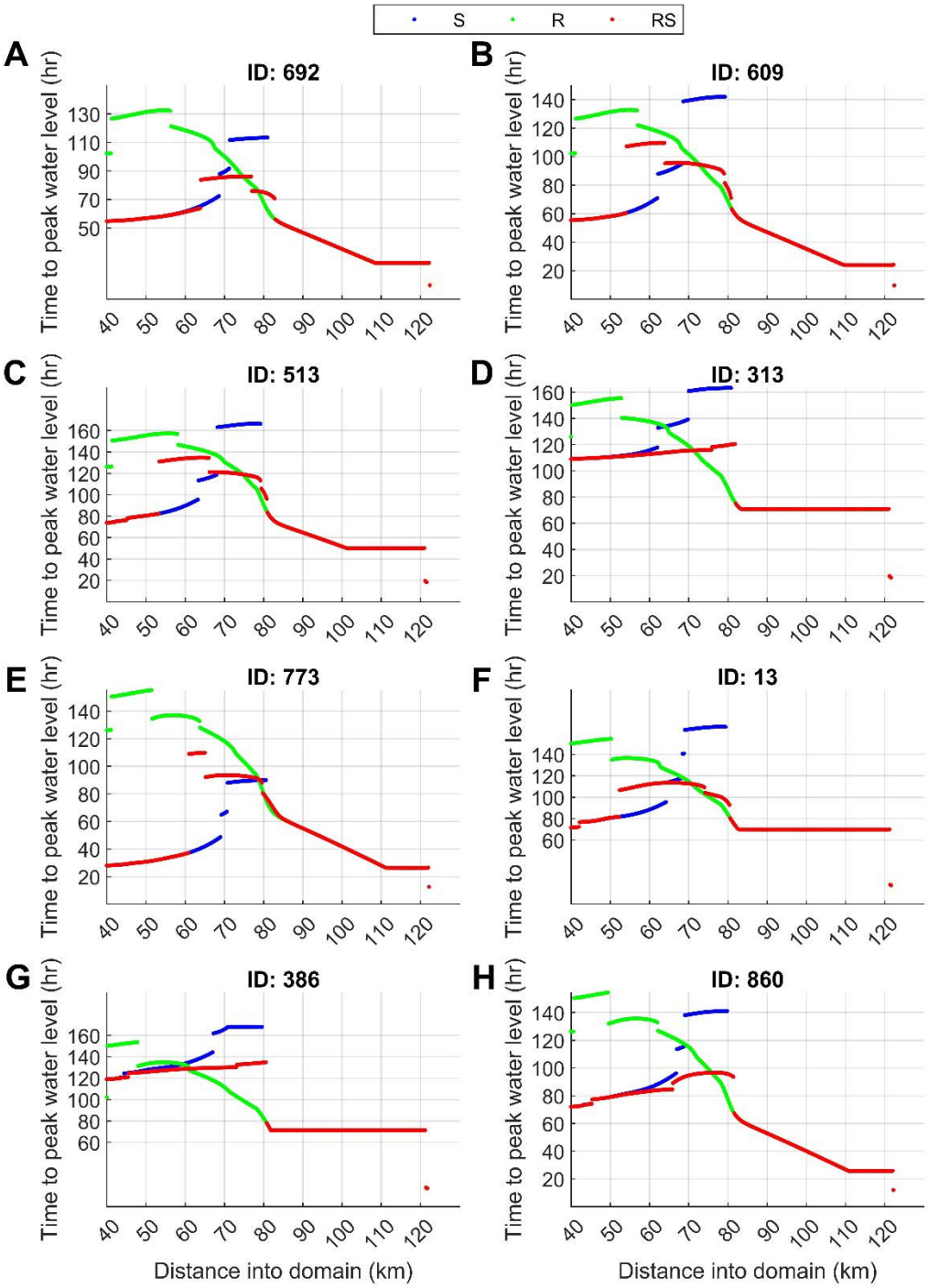

Figure 5. Time to peak water level for different flooding scenarios of the simulation subset. The blue, green, and red dots represent the storm surge only (S), rainfall-runoff only (R), and combined flood (RS) scenarios, respectively. The title of each subpanel refers to the simulation ID within the subset. (created using MATLAB)

775 The descriptive statistics and the relative probability of the MWL were computed for
776 each simulation under the three flooding scenarios (Figure 6). For the S scenario, the mean
777 MWL occurs at the middle segment's beginning and decreases as it extends through this segment
778 (Figure 6a). For example, 68% of the MWL, which represents +/- one standard deviation from
779 the mean, are within 1.14 and 1.90 m at the middle segment's beginning but decreases to 0.39
780 and 0.49 at the end of this segment. This behavior is expected since the MWLs, due to the storm
781 surge flooding mechanism, occur at shallow bathymetric depths and decrease as they move
782 inland due to flow resistance and gravity. For the R scenario, the mean MWL at the upper
783 segment is less than at the middle segment, even though the rainfall falls directly over the upper
784 segment (Figure 6c). This behavior is mainly due to gravity that accelerates the freshwater flow
785 over steeper slopes, such as the upper segment, preventing the water levels from increasing
786 rapidly. When the high-velocity freshwater flow reaches a milder slope like the middle segment,
787 the water levels have to increase to compensate for the slower velocities, thereby conserving
788 mass as governed by the continuity equation. For the RS scenario, the MWL at the beginning of
789 the middle segment and throughout the lower segment is mainly driven by coastal processes
790 since these values overlap with the ones from the S scenario (Figure 6e). Conversely, the MWLs
791 beyond 81 km into the domain are mainly driven by hydrologic processes since these values
792 overlap with ones from the R scenario. Therefore, the total water levels at the middle segment
793 and the first 3 km of the upper segment are influenced by both flooding mechanisms, on average,
794 during a compound flood event.

795 Similarly, the descriptive statistics and the relative probability of the TPWLs illustrate
796 that the range of 68% of the TPWLs remains relatively constant (within 1 hr) throughout the
797 middle segment with a value of 40 hr for the S scenario. This behavior represents that the spatial
798 variation of the TPWLs is mainly dominated by the flow resistance parameters and not by the
799 variations in input parameters since Manning's roughness is constant throughout each segment
800 for this case study. Three different periods were identified with the highest (> 5%) relative
801 probability of peak water levels in the middle segment (Figure 6b). These three periods
802 approximately equal (within 1 hr) the time between successive high tides (24 hr), meaning that
803 the astronomical tides flooding mechanism regularly influences the TPWLs for the S scenario.
804 This behavior also occurs in the R scenario for the first 12 km of the middle segment. For the RS
805 scenario, the TPWLs for the first 10 km of the middle segment overlap the ones from the S
806 scenario, while most (89%) of the upper segment overlap the ones from the R scenario.
807 Therefore, there is a 34 km region where both flooding mechanisms, on average, influence the
808 compound flood's timing and have some of the highest (> 6%) relative probability of occurrence.
809 This behavior represents that the most frequent TPWL occurs at the region where both flooding
810 mechanisms influence the total water level, highlighting the importance of using a compound
811 flood modeling approach to assess multi-hazard flood events at coastal watersheds.

812

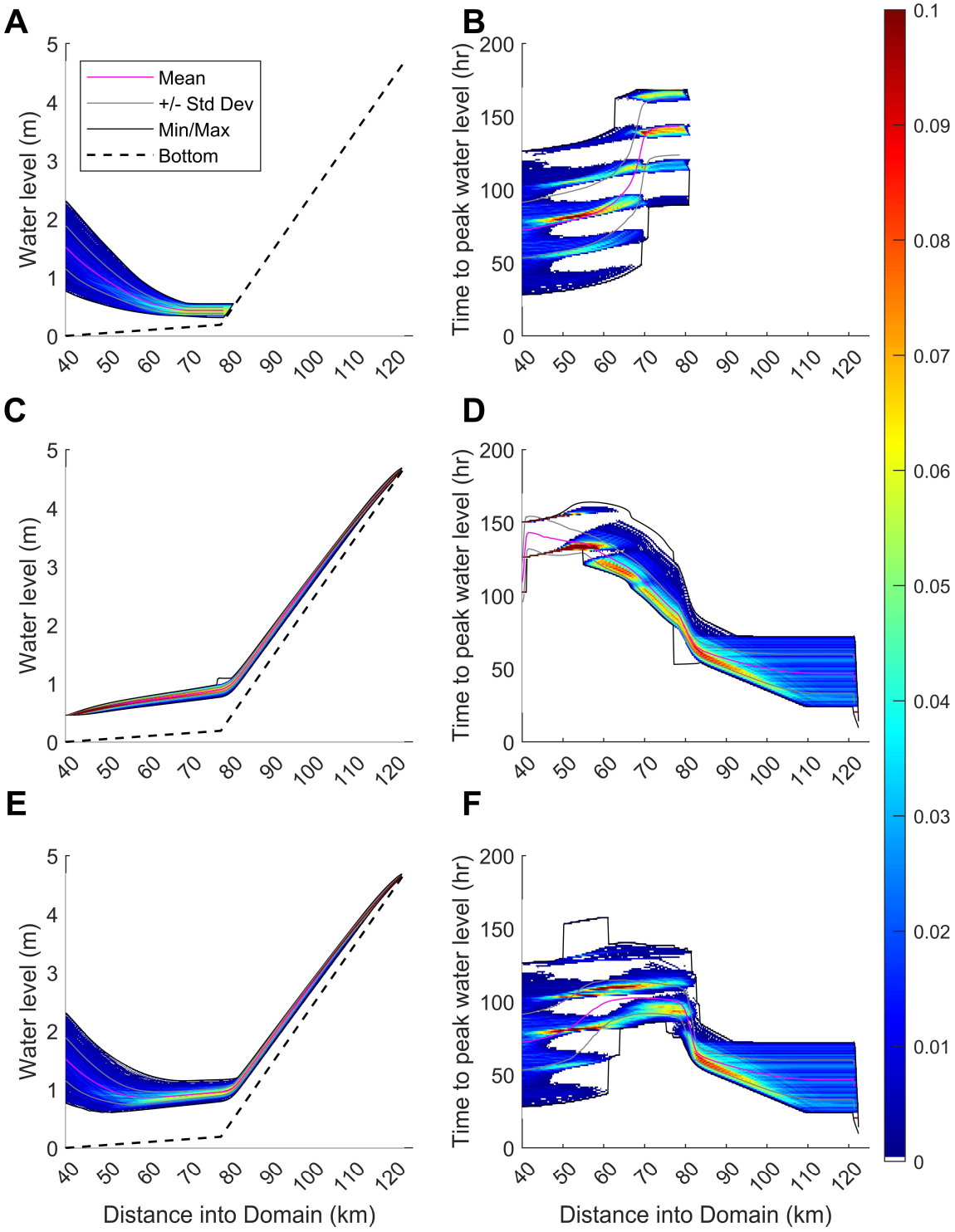
A
B
C
D
E
F
Mean
+/- Std Dev
Min/Max
Bottom
Water level (m)
Time to peak water level (hr)
Distance into Domain (km)
0
1
2
3
4
5
0
50
100
150
200
40
50
60
70
80
90
100
110
120
0.1
0.09
0.08
0.07
0.06
0.05
0.04
0.03
0.02
0.01
0

813

Figure 6. Maximum water levels (a,c,e) and time to peak water level (b,d,f) for the complete set of simulations under different flooding scenarios: (a,b) storm surge only, (c,d) rainfall-runoff only, and (e,f) combined flood. The color bar on the right corresponds to the relative probability. (created using MATLAB)

4.3 Compound Flood Hazard Zones

The compound flood hazard zones (FHZs) were delineated for the entire simulation set (Figure 7). These FHZs were classified into hydrologic, transition, and coastal. Results from the simulation's subset (Figure 7A) illustrate that the extent of the compound FHZs is directly proportional to the forcing's magnitude. For example, a higher storm surge event (Simulation 692) results in a larger coastal FHZ than smaller events (Simulation 609). A similar trend was observed for the forcing's timing only, such as Simulation 13 vs. 386. However, when considering the forcing's magnitude and timing, the relationship with the extent of the compound FHZ is not proportional. For example, the coastal FHZ of Simulation 773 is 50% greater than the one for Simulation 313, despite the fact that Simulation 313 has a greater peak storm surge level and lager time between the rainfall event and the peak storm surge than Simulation 773. Furthermore, the nonlinearity of both flooding mechanisms can be demonstrated through the compound FHZ. For example, high rainfall events (320 mm total rain) could produce smaller hydrologic FHZs than small rainfall events (229 mm total rain), mainly because the transition FHZ increases due to large peak levels and time-to-peak storm surge events, such as Simulation 313 vs. 513.

The coastal and hydrologic interfaces were computed for the entire simulation set to determine the relative probability of where these FHZs begin or end (Figure 7b). The coastal interface refers to the location where the coastal FHZ ends and the transition FHZ begins. In contrast, the hydrologic interface refers to the end of the transition FHZ and the beginning of the hydrologic FHZ. The minimum, mean, and maximum coastal interfaces are 39.2, 46.7, and 61.8 km into the domain, respectively, while the hydrologic interfaces are 72.8, 80.8, and 83.2. Therefore, the transition flood hazard zone extends from 46.7 to 80.8 km into the domain on average. These findings represent that coastal processes can influence the total water levels up to 41 km inland under a compound inundation event for this idealized transect. The coastal interface has its highest (> 10%) relative probability of occurrence between 40.6 to 47 km into the domain, while the hydrologic interface occurs between 79.7 to 82.5 km into the domain. Therefore, the transition flood hazard zone with the highest relative probability of occurrence extends from 40.6 to 82.5 km into the domain. These results represent a high relative probability that the coastal processes dominate the total water levels up to 42.5 km into the domain, while the hydrologic processes dominate beyond 82.5 km during a compound flood event.

The length of the compound FHZs was determined for the complete simulation set (Figure 7C). The minimum and mean lengths for the coastal and hydrologic FHZs were very similar, with 39.2 and 46.7 km for the coastal FHZ, respectively, and 39.8 and 42.2 km for the hydrologic FHZ, respectively. However, their maximum coastal FHZ was 11.6 km longer than the hydrologic one. On the other hand, the minimum, mean, and maximum transition FHZ was significantly less, with 21.4, 34.1, and 41.6 km, respectively. There is a high (> 20%) relative probability that both the coastal and hydrologic FHZs have a similar length, between 41-42 km. Conversely, the most probable length for the transition FHZ is 5 km smaller than the other two FHZs. When plotted together, both the coastal and transition FHZs have a more extensive spread

858 in their distribution rather than a centralized distribution as the hydrologic one. These findings
859 represent that, on average, each flooding mechanism dominates the total water levels at larger
860 portions of the domain than both having an influence within the same region during a compound
861 inundation event.

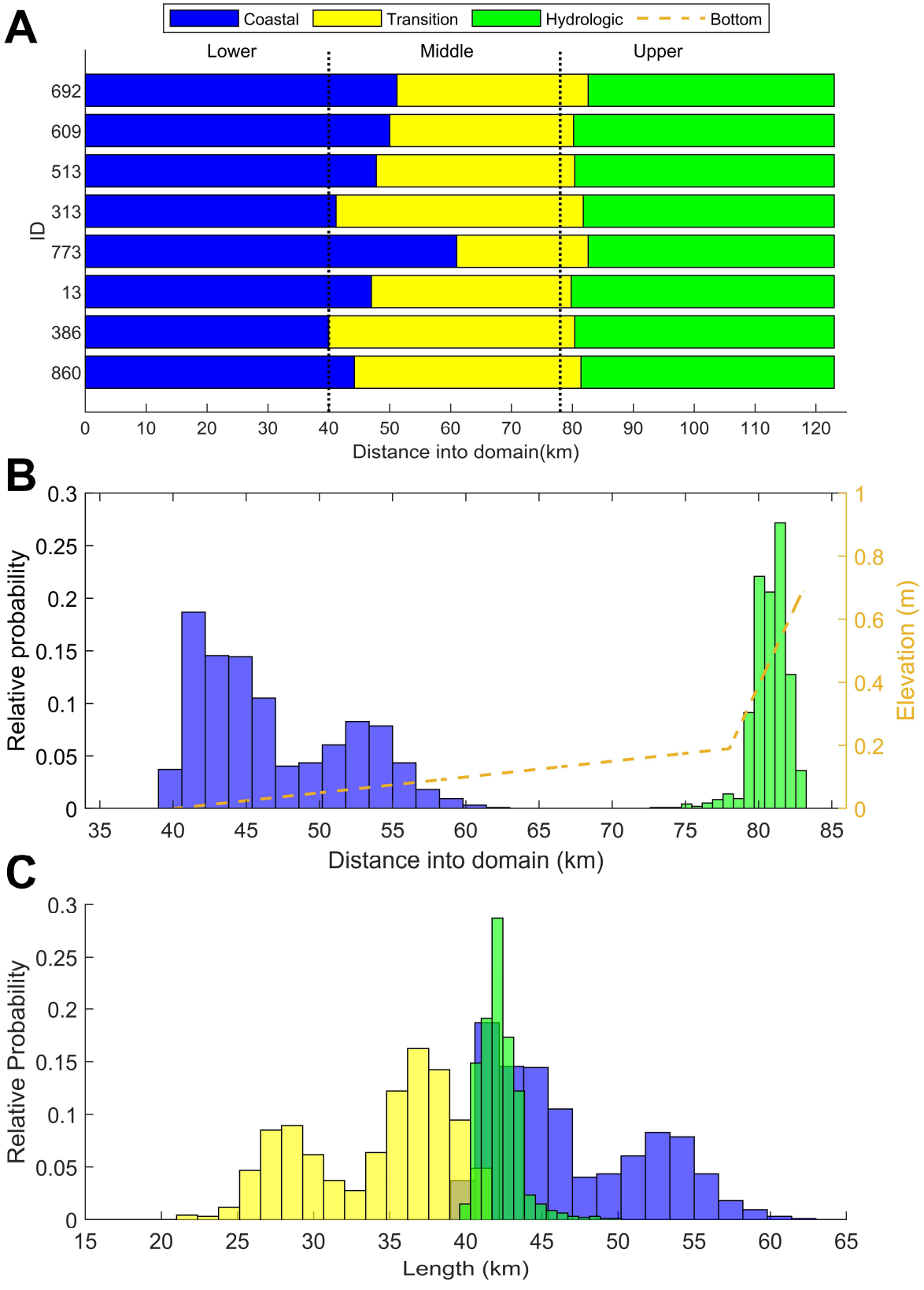
A
Coastal
Transition
Hydrologic
Bottom
Lower
Middle
Upper
692
609
513
313
773
13
386
860
ID
0 10 20 30 40 50 60 70 80 90 100 110 120
Distance into domain(km)
B
Relative probability
0 0.05 0.1 0.15 0.2 0.25 0.3
Elevation (m)
0 0.2 0.4 0.6 0.8 1
35 40 45 50 55 60 65 70 75 80 85
Distance into domain (km)
C
Relative Probability
0 0.05 0.1 0.15 0.2 0.25 0.3
15 20 25 30 35 40 45 50 55 60 65
Length (km)

862
863

Figure 7. Compound flood hazard zones for the simulation subset (a), and relative probability of the compound flood hazard zone's (b) interface and (c) lengths for the entire simulation set. Each color bar represents a different compound flood hazard zone. The gold dashed line represents the idealized coastal watershed transect. The dotted lines represent the different segments within the idealized coastal watershed transect. (created using MATLAB)

4.4 Governing Input Parameters

The weighting parameters from the severity index (SI) equation (Eq. 10) were computed based on all the simulation results at different regions of interest to investigate the influence of each input parameter in the compound inundation levels. The regions selected are the compound FHZ, the different domain segments, and the entire domain. Results from the ordinary least-square regression show that there is a similarity in the computed weighting parameters between the compound FHZs and the domain segments (Figure 8). For example, the transition FHZ and the middle segment have similar weighting parameter values. The same behavior occurs between the coastal FHZ and the lower segment, and the hydrologic FHZ and the upper segment. Thus, compound FHZs depend not only on the environmental forcings but also on the domain characteristics. In other words, the ground elevation (including the slope) and roughness influence the FHZs. Furthermore, based on the weighting parameters, the SI can be used as an initial estimate of compound FHZ's location.

At the lower segment/coastal FHZ, the storm surge magnitudes significantly dominate the inundation level, with more than 50% of the total contribution of the total weighting factors (Figure 8B-C). This behavior represents that the coastal processes dominate this region. Surprisingly, the hydrologic parameters have a greater weight than the time-related parameters of the coastal processes at these locations. Furthermore, the total contribution of the coastal processes time parameters is not even 4% and 8% for the coastal FHZ and lower segment, respectively. Thus, the hydrologic parameters have a greater influence on the coastal FHZ than on the lower segment. This behavior is expected since the coastal FHZ penetrates up to 7km inland, on average, while the lower segment does not.

At the middle segment/transition FHZ, only three parameters (out of five) comprise the SI (Figure 8D-E). Two are related to hydrologic processes and account for more than 66% of the flooding at these locations. This represents that the dominant factor within this region is the hydrologic processes. Unexpectedly, the coastal time parameters do not contribute to the SI in this region, meaning that the storm surge arrival could fluctuate without affecting the SI. Also, these regions reported the highest coefficient of determination (R^2) and lowest root-mean-square error (RMSE) with an R^2 of 0.68 and 0.62 and an RMSE of 0.06 and 0.07 for the transition FHZ and middle segment, respectively (Figure S7). This behavior is expected since both flooding mechanisms have a greater opportunity to co-occur at these locations. Note that the RMSE was obtained from a linear regression on the flood rank vs. the SI, in which the flood rank is the abscissa and the SI the ordinate.

At the upper segment/hydrologic FHZ, all parameters contribute to the SI (Figure 8E-F). As expected, the dominant factor is the hydrologic processes with up to 65% of the total parameters. However, coastal process time parameters have a more significant contribution in the upper segment than in the lower and middle segments. Also, the time between peak storm surge a high tide has a similar (within 2%) weight in the SI. Therefore, the coastal time parameters play a role in the penetration of seawater inland at higher elevations.

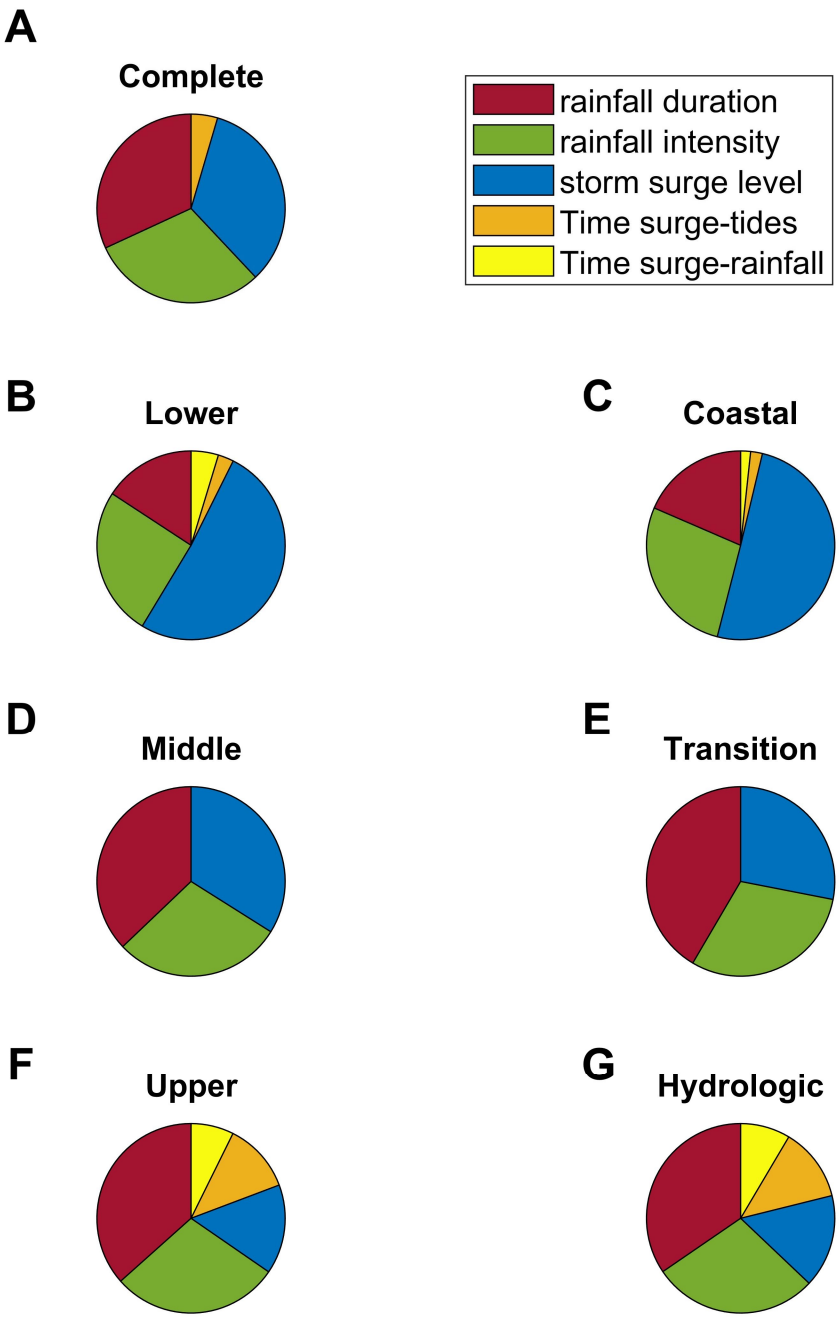

908

909 **Figure 8**. Weighting parameters of the severity index for the complete set of simulations at
910 different locations: (a) complete domain, (b) lower segment, (c) coastal FHZ, (d) middle
911 segment, (e) transition FHZ, (f) upper segment, and (g) hydrologic FHZ. The different colors

represent the weighting parameters in the severity index equation (Eq. 10). (created using MATLAB)

5 Discussion

Compound inundation can vary widely due to several factors, such as coastal watershed characteristics (e.g., bathymetry / topography and LULC), environmental forcings (e.g., storm surge, rainfall, and astronomical tides), and the timeline of weather events. In general, the astronomical tide flooding mechanisms dominate the water levels across the middle segment before combining with the rainfall-runoff flooding mechanism, which controls the water levels at the upper segment. Then, the total water levels at the middle segment are dominated by the rainfall-runoff flooding mechanism, with its maximum contribution occurring after the antecedent rainfall event ends. As the peak storm surge approaches the middle segment, the water levels at the middle segment are influenced by both coastal and hydrologic processes. The inland penetration of the storm surge depends on several factors, such as surface roughness, bathymetry / topography, and astronomical tides, but in a compound inundation event, the momentum of each flooding mechanism must be considered. When the freshwater momentum is greater than the seawater momentum, the rainfall-runoff attenuates the storm surge effects, especially at farther inland locations. For example, the mean seawater momentum (S scenario) that penetrates inland through the middle segment is 1,811 kg m s^{-1} for Simulation 692, while the compound momentum (RS scenario) is 6,222 kg m s^{-1}, but moving seaward. Thus, the mean relative change in momentum (see more details in Text S6) is 55%, which represents that the rainfall-runoff contributed, on average, up to double the amount of momentum to attenuate the storm surge effects during a compound inundation event. Similar behavior was observed for the other simulations within the subset, with an average for the subset of 86% (Figure S8). This momentum exchange is often neglected due to the lack of a tightly- or fully-coupled approach between both flooding mechanisms (Bakhtyar et al., 2020b; Orton et al., 2018). Therefore, the velocity component of each flooding mechanism should be considered in any compound inundation event using a tightly- or fully-coupled approach. This is a major shortcoming in using a superposition approach or inappropriate coupling.

Compound inundation levels are affected by both the environmental forcing's magnitude and timing. At the coastal FHZ, the magnitude of the storm surge flooding mechanisms dominates the total water levels, being the major parameter contributing to the SI. On the contrary, the magnitude and time of the rainfall-runoff flooding mechanisms dominate the total water levels at the hydrologic FHZ, being over two times more significant (based on the weighting parameters of the SI) than the storm surge flooding mechanisms at this location. However, each flooding mechanism's contribution (e.g., magnitude only) to the total water levels at the transition FHZ is more evenly distributed than the other FHZs. This behavior suggests that the timing of each flooding mechanism substantially influences the compound inundation levels, especially within the hydrological FHZ. Surprisingly, this is not supported for the transition FHZ, as other studies have stated (Tanim & Goharian, 2021; Hsiao et al., 2021). Furthermore, the proposed SI can be a faster alternative approach to identifying the compound flood hazard zone since it only requires one-third of the total simulations than the maximum water level profile approach.

Overall, the synchronization of the coastal processes substantially impacts the SI and the compound inundation. For example, the time between the peak storm surge and high

astronomical tide levels can greatly affect the total water levels due to the non-linear interaction (Tanim & Goharian, 2021; Terry et al., 2021), especially at the hydrologic FHZ. If the astronomical tide flooding mechanisms are not considered, the *worst case* (i.e., all input parameters are at their maximum value) simulation has a lower Flood Rank ($\overline{F_R} = 0.8$) than other simulations (e.g., $\overline{F_R} = 0.83$ for Simulation 90) at the hydrologic FHZ, despite having a higher SI (1 vs. 0.62). This behavior can be attributed to the substantial importance the timing of the coastal processes has in the compound flood levels, especially at the hydrologic FHZ. The astronomical tides flooding mechanism influences the time to peak water levels for the storm surge only and rainfall-runoff only scenario at the upper segment, having up to 10% of contribution in this location. Thus, the astronomical tides provide an important non-linear contribution to the compound flood hazard and should be included as a flooding mechanism in any compound inundation study.

In general, the total water levels throughout the lower segment are mainly driven by coastal processes, while the upper segment is primarily driven by hydrologic processes. However, the middle segment's total water levels are influenced by coastal and hydrologic processes (i.e., transition FHZ). In locations where the maximum water levels from both flooding mechanisms coincide, the linear superposition of these individual flood levels overestimates the total water level, leading to larger errors versus considering them in the same simulation (Huang et al., 2021). Thus, the existence of a non-linear relationship between the astronomical tides, storm surge, and rainfall-runoff is evident in a compound inundation event (Bilskie et al., 2021; Bilskie & Hagen, 2018) and may even increase its non-linearity levels in future scenarios as a result of climate change and anthropogenic effects (Santiago-Collazo et al., 2021; Xu et al., 2023). Regarding relative probability for the case study, the coastal FHZ is most likely to end between 39.4 to 61.8 km, while the hydrologic FHZ is most likely to start between 72.8 to 83.2 km into the domain. Therefore, the transition flood hazard zone can span throughout the three segments of the domain, covering the entire middle segment and up to 4 km of the upper segment, and is where the most frequent time to peak water level occurs. Hence, the compounding effects of multiple flood mechanisms should be considered when developing compound flood hazard maps, especially in low-gradient coastal land-margin (Zhang & Najafi, 2020).

6 Conclusions

This study presents a 1-D inundation model capable of assessing the physical interaction between various flooding mechanisms (i.e., storm surge, rainfall-runoff, and astronomical tides) through a reduced physics approach. The modeling framework consists of three separate modules (i.e., Coastal, Watershed, and Overland Hydraulics Modules) based on the same fundamental equations that are being simplified for certain flooding mechanisms, such as the kinematic wave equations for hydrologic processes or the shallow water equations for coastal processes. A single wetting and drying algorithm was applied to all three modules to reduce numerical instabilities. The modules that compose this modeling framework and the coupling technique between them were verified against analytical solutions and mass balance analysis. Based on observed data, an idealized coastal watershed transect was developed to test thousands of combinations of flooding mechanisms at a low computational cost. This modeling framework created maximum water level profiles, delineated compound FHZs, and developed a SI of the compound inundation.

The velocity component of each flood mechanism can substantially impact the total water levels by attenuating the storm surge inland penetration or exacerbating the rainfall-runoff inundation due to backwater effects. This component should be considered in any compound flood study regarding discharge since it provides valuable insight into the flow direction and momentum exchange of each flooding mechanism. Compound inundation levels are affected by the magnitude and timing of each flooding mechanism, especially in the transition FHZ, where both flooding mechanisms influence the total water levels. The SI can be an alternative approach to select the most critical combinations of flooding mechanisms at different domain locations before executing any simulation. The proposed study may serve as an initial attempt to describe the interaction between the flooding mechanisms, as well as to establish guidelines for delineating compound FHZs. Also, a 1D modeling framework can aid in developing flood frequency analysis for compound flood events due to its low computational cost and fast assembly. Therefore, researchers, engineers, and stakeholders can move towards better flood resiliency practices, such as flood hazard maps for compound events, that can aid planning and management of low-gradient coastal land-margins.

The lessons learned from this 1-D inundation model may serve as a foundation for future endeavors to build upon when developing 2-D models to improve compound flood assessments. This holistic modeling approach can be accomplished by considering different approximations of the St. Venant equations to characterize the different types of surface flow. Future efforts will focus on applying the proposed 1-D modeling framework at a larger spatial scale (nationally or globally) to aid in identifying low-gradient coastal land-margins based on physics-based parameters and idealized transects that represent different coastal watersheds which were not included in this study. These regions are prone to compound flood impacts, and their low-gradient profile may exacerbate the flooding effects. A tool that identifies these compound flood hotspots can help focus future efforts, such as comprehensive (i.e., 2-D modeling approach) compound flood analysis, where they are needed most. Thus, enhancing coastal resilience measures and supporting authorities, stakeholders, and policy-makers in their quest to understand present and future consequences, evaluate risk and ultimately mitigate compound flooding effects through science and more informed engineering practices.

Acknowledgments

This research was initially performed in the Department of Civil and Environmental Engineering at Louisiana State University and completed at the University of Georgia. This material is based upon work supported in part by the National Science Foundation Graduate Research Fellowship Program [grant number 1452778]; the Department of the Treasury through the Louisiana Coastal Protection and Restoration Authority's Center of Excellence Research Grants Program under the Resources and Ecosystems Sustainability, Tourist Opportunities, and Revived Economies of the Gulf Coast States Act of 2012 (RESTORE Act) [grant number CPRA-2015-COE-MB]; the Gulf Research Program (GRP) of the National Academies of Sciences, Engineering, and Medicine [grant number 200000829]; the Robert Wood Johnson Foundation (RWJF) [grant number 200000829], and the Louisiana Sea Grant Laborde Chair.

The authors greatly appreciated the help provided by Dr. Jin Ikeda during the verification of the Coastal Hydraulics Module. Model simulations were conducted on the University of Georgia Advanced Resource Computing Resource Center (GACRC) Sapelo2 High-Performance

Computing (HPC) Cluster, and the HPC at Louisiana State University (LSU) and the Louisiana Optical Network Initiative (LONI). Any opinions, findings, conclusions, or recommendations expressed in this material are those of the author(s) and do not necessarily reflect the views of the NSF, the Department of Treasury, GRP, RWJF, GACRC, LSU, LONI, or the Louisiana Sea Grant College Program.

Open Research

Harmonic constituents for the different tidal gauges across Louisiana were obtained from NOAA Tides and Currents (NOAA, 2021). Rainfall frequency quantiles were obtained from NOAA's Atlas 14 (Bonnin et al., 2006). Maximum water level profiles for each simulation under each flooding scenario are available at FigShare (Santiago-Collazo et al., 2021b).Time to peak water levels profiles for each simulation under each flooding scenario, are available at FigShare (Santiago-Collazo et al., 2021c). The different combinations of the environmental forcing parameters created using the Random Sampling Technique are available at FigShare (Santiago-Collazo et al., 2021d). The compound inundation modeling framework developed in this research is freely available on Zenodo (Santiago-Collazo et al., 2023).

References

Bacopoulos, P., Tang, Y., Wang, D., & Hagen, S. C. (2017). Integrated Hydrologic-Hydrodynamic Modeling of Estuarine-Riverine Flooding: 2008 Tropical Storm Fay. *Journal of Hydrologic Engineering*, *22*(8), 04017022. https://doi.org/10.1061/(ASCE)HE.1943-5584.0001539

Bakhtyar, R., Maitaria, K., Velissariou, P., Trimble, B., Mashriqui, H., Moghimi, S., et al. (2020a). A New 1D/2D Coupled Modeling Approach for a Riverine-Estuarine System Under Storm Events: Application to Delaware River Basin. *Journal of Geophysical Research: Oceans*, *125*(9). https://doi.org/10.1029/2019JC015822

Bakhtyar, R., Maitaria, K., Velissariou, P., Trimble, B., Mashriqui, H., Moghimi, S., et al. (2020b). A New 1D/2D Coupled Modeling Approach for a Riverine-Estuarine System Under Storm Events: Application to Delaware River Basin. *Journal of Geophysical Research: Oceans*, *125*(9). https://doi.org/10.1029/2019JC015822

Bensi, M., Mohammadi, S., Kao, S.-C., & Deneale, S. T. (2020). *Multi-Mechanism Flood Hazard Assessment : Critical Review of Current Practice and Approaches*. Oak Ridge, TN.

Bilskie, Matthew v, Zhao, H., Resio, D., Atkinson, J., Cobell, Z., & Hagen, S. (2021). Enhancing Flood Hazard Assessments in Coastal Louisiana through Coupled Hydrologic and Surge Processes. *Frontiers in Water*, *3*, 1–19. https://doi.org/10.3389/frwa.2021.6092311

Bilskie, M. v., & Hagen, S. C. (2018). Defining Flood Zone Transitions in Low-Gradient Coastal Regions. *Geophysical Research Letters*, *45*(6), 2761–2770. https://doi.org/10.1002/2018GL077524

Blanton, B., Dresback, K., Colle, B., Kolar, R., Vergara, H., Hong, Y., et al. (2018). An Integrated Scenario Ensemble-Based Framework for Hurricane Evacuation Modeling:Part 2—Hazard Modeling. *Risk Analysis*, *00*(00). https://doi.org/10.1111/risa.12990

Bonnin, G. M., Martin, D., Lin, B., Parzybok, T., Yekta, M., & Riley, D. (2006). *NOAA Atlas 14: Precipitation-Frequency Atlas of the United States*. Silver Spring, MD.

Brufau, P., García-Navarro, P., & Vázquez-Cendón, M. E. (2004). Zero mass error using unsteady wetting-drying conditions in shallow flows over dry irregular topography. *International Journal for Numerical Methods in Fluids*, *45*(10), 1047–1082. https://doi.org/10.1002/fld.729

Carrier, G. F., & Greenspan, H. P. (1958). Water waves of finite amplitude on a sloping beach. *Journal of Fluid Mechanics*, *4*(1), 97–109.

Chen, C., Tsai, C., Wu, M., & Tsai, C. (2013). Numerical simulation of potential inundation in a coastal zone. *Journal of Flood Risk Management*, *8*, 208–223. https://doi.org/10.1111/jfr3.12088

Cheng, J. C., Hunter, R. M., & Lin, H. (2010). *Demonstration of a Coupled Watershed-Nearshore Model*. Vicksburg,MS.

Chen, W. B., & Liu, W. C. (2014). Modeling flood inundation induced by river flow and storm surges over a river basin. *Water (Switzerland)*, *6*(10), 3182–3199. https://doi.org/10.3390/w6103182

Cifelli, R., Johnson, L. E., Kim, J., Coleman, T., Pratt, G., Herdman, L., et al. (2021). Assessment of flood forecast products for a coupled tributary-coastal model. *Water (Switzerland)*, *13*(3), 1–24. https://doi.org/10.3390/w13030312

Comer, J., Indiana Olbert, A., Nash, S., & Hartnett, M. (2017). Development of high-resolution multi-scale modelling system for simulation of coastal-fluvial urban flooding. *Natural Hazards and Earth System Sciences*, *17*(2), 205–224. https://doi.org/10.5194/nhess-17-205-2017

Van Cooten, S., Kelleher, K. E., Howard, K., Zhang, J., Gourley, J. J., Kain, J. S., et al. (2011). The CI-flow project: A system for total water level prediction from the summit to the sea. *Bulletin of the American Meteorological Society*, *92*(11), 1427–1442. https://doi.org/10.1175/2011BAMS3150.1

Costabile, P., Costanzo, C., & MacChione, F. (2013). A storm event watershed model for surface runoff based on 2D fully dynamic wave equations. *Hydrological Processes*, *27*(4), 554–569. https://doi.org/10.1002/hyp.9237

Dietrich, J. C., Kolar, R. L., & Luettich, R. A. (2004). Assessment of ADCIRC's wetting and drying algorithm. In *Computational Methods in Water Resources: Proceedings of the XVth International Conference on Computational Methods in Water Resources* (pp. 1767–1778). https://doi.org/10.1016/S0167-5648(04)80183-7

Dietrich, J. C., Kolar, R. L., & Westerink, J. J. (2005). Refinements in Continuous Galerkin Wetting and Drying Algorithms. In *Estuarine and Coastal Modeling: Proceedings of the 9th International Conference* (pp. 637–656). Charleston, SC.

Dietrich, J. C., Kolar, R. L., & Dresback, K. M. (2008). Mass Residuals as a Criterion for Mesh Refinement in Continuous Galerkin Shallow Water Models. *Journal of Hydraulic Engineering*, *134*(5), 520–532. https://doi.org/10.1061/(asce)0733-9429(2008)134:5(520)

Dresback, K. M., & Kolar, R. L. (2001). An implicit time-marching algorithm for shallow water models based on the generalized wave continuity equation. *International Journal of Numerical Methods in Fluids*, *36*, 925–945. https://doi.org/10.1002/fld.157

Dresback, K. M., Kolar, R. L., & Dietrich, J. C. (2004). A 2D implicit time-marching algorithm for shallow water models based on the generalized wave continuity equation. *International Journal for Numerical Methods in Fluids*, *45*(3), 253–274. https://doi.org/10.1002/fld.697

Dresback, K. M., Fleming, J. G., Blanton, B. O., Kaiser, C., Gourley, J. J., Tromble, E. M., et al. (2013). Skill assessment of a real-time forecast system utilizing a coupled hydrologic and coastal hydrodynamic model during Hurricane Irene (2011). *Continental Shelf Research*, *71*, 78–94. https://doi.org/10.1016/j.csr.2013.10.007

Faiers, G. E., Keim, B. D., & Muller, R. A. (1997). *Rainfall Frequency/Magnitude Atlas for the SouthCentral United States: SRCC Technical Report 97-1 Geoscience*. Baton Rouge, LA.

FEMA, & USACE. (2008). *Flood Insurance Study: Southeastern Parishes, Louisiana, Intermediate Submission 2: Offshore Water Levels and Wave Rep.*

Fiedler, F. R., & Ramirez, J. A. (2000). A numerical method for simulating discontinuous shallow flow over an infiltrating surface. *International Journal for Numerical Methods in Fluids*, *32*(2), 219–239. https://doi.org/10.1002/(SICI)1097-0363(20000130)32:2<219::AID-FLD936>3.0.CO;2-J

Fleming, E., Payne, J., Sweet, W., Craghan, M., Haines, J., Hart, J. F., et al. (2018). Coastal Effects. In *Impacts, Risk, and Adaptation in the United States: Foruth National Climate Assessment, Volume II* (pp. 322–352). Washington, DC: US Global Change Research Program. https://doi.org/10.7930/NCA4.2018.CH3

Ganguli, P., Paprotny, D., Hasan, M., Güntner, A., & Merz, B. (2020). Projected Changes in Compound Flood Hazard From Riverine and Coastal Floods in Northwestern Europe. *Earth's Future*, *8*(11). https://doi.org/10.1029/2020EF001752

Gori, A., Lin, N., & Smith, J. (2020). Assessing Compound Flooding From Landfalling Tropical Cyclones on the North Carolina Coast. *Water Resources Research*, *56*(4). https://doi.org/10.1029/2019WR026788

Gori, A., Lin, N., & Xi, D. (2020). Tropical cyclone compound flood hazard assessment: from investigating dependence to quantifying impacts.*Earth's Future*, 8, e2020EF001660. https://doi.org/ 10.1029/2020EF001660

Gottardi, G., & Venutelli, M. (1993). A control-volume finite-element model for two-dimensional overland flow. *Advances in Water Resources*, *16*, 277–284.

Haddad, K., Rahman, A., & Kuczera, G. (2011). Comparison of ordinary and generalis ed least squares regression models in regional flood frequency analysis: A case study for New South Wales. *Australian Journal of Water Resources*, *15*(1), 59–70. https://doi.org/10.1080/13241583.2011.11465390

Haddad, Khaled, Rahman, A., A Zaman, M., & Shrestha, S. (2013). Applicability of Monte Carlo cross validation technique for model development and validation using generalised least squares regression. *Journal of Hydrology*, *482*, 119–128. https://doi.org/10.1016/j.jhydrol.2012.12.041

Hasan Tanim, A., & Goharian, E. (2021). Developing a hybrid modeling and multivariate analysis framework for storm surge and runoff interactions in urban coastal flooding. *Journal of Hydrology*, *595*(March 2020), 125670. https://doi.org/10.1016/j.jhydrol.2020.125670

Hewageegana, V. H., Bilskie, M. V., Woodson, C. B., & Bledsoe, B. P. (2022). The effects of coastal marsh geometry and surge scales on water level attenuation. Ecological Engineering, 185(August), 106813. https://doi.org/10.1016/j.ecoleng.2022.106813

Hsiao, S. C., Chiang, W. S., Jang, J. H., Wu, H. L., Lu, W. S., Chen, W. B., & Wu, Y. T. (2021). Flood risk influenced by the compound effect of storm surge and rainfall under climate change for low-lying coastal areas. *Science of the Total Environment*, *764*, 144439. https://doi.org/10.1016/j.scitotenv.2020.144439

Huang, W., Ye, F., Zhang, Y. J., Park, K., Du, J., Moghimi, S., et al. (2021). Compounding factors for extreme flooding around Galveston Bay during Hurricane Harvey. *Ocean Modelling*, *158*, 101735. https://doi.org/10.1016/j.ocemod.2020.101735

Ikeuchi, H., Hirabayashi, Y., Yamazaki, D., Muis, S., Ward, P. J., Winsemius, H. C., et al. (2017). Compound simulation of fluvial floods and storm surges in a global coupled river-coast flood model: Model development and its application to 2007 Cyclone Sidr in Bangladesh. *Journal of Advances in Modeling Earth Systems*, *9*(4), 1847–1862. https://doi.org/10.1002/2017MS000943

Kazezyilmaz-Alhan, C. M., Medina, M. A., & Rao, P. (2005). On numerical modeling of overland flow. *Applied Mathematics and Computation*, *166*(3), 724–740. https://doi.org/10.1016/j.amc.2004.06.063

Keim, B. D., & Faiers, G. E. (2000). A comparison of techniques to produce quantile estimates of heavy rainfall in arid and mountainous environments: A test case in western Texas. *Journal of Arid Environments*, *44*(3), 267–275. https://doi.org/10.1006/jare.1999.0599

Kinnmark, I. (1986). *The Shallow Water Wave Equations: Formulation, Analysis and Application*. Ne: Springer-Verlag.

Kolar, R. L., Westerink, J. J., Cantekin, M. E., & Blain, C. A. (1994). Aspects of nonlinear simulations using shallow-water models based on the wave continuity equation. *Computers and Fluids*, *23*(3), 523–538. https://doi.org/10.1016/0045-7930(94)90017-5

Lall, U., Johnson, T., Colohan, P., Aghakouchak, A., Brown, C., McCabe, G., et al. (2018). Water. In *Impacts, Risk, and Adaptation in the United States: Foruth National Climate Assessment, Volume II* (pp. 145–173). Washington, DC: US Global Change Research Program. https://doi.org/10.7930/NCA4.2018.CH3

Lee, C., Hwang, S., Do, K., & Son, S. (2019). Increasing flood risk due to river runoff in the estuarine area during a storm landfall. *Estuarine, Coastal and Shelf Science*, *221*(February), 104–118. https://doi.org/10.1016/j.ecss.2019.03.021

Leijnse, T., van Ormondt, M., Nederhoff, K., & van Dongeren, A. (2021). Modeling compound flooding in coastal systems using a computationally efficient reduced-physics solver: Including fluvial, pluvial, tidal, wind- and wave-driven processes. *Coastal Engineering*, *163*(December 2019), 103796. https://doi.org/10.1016/j.coastaleng.2020.103796

Loveland, M., Kiaghadi, A., Dawson, C. N., Rifai, H. S., Misra, S., Mosser, H., & Parola, A. (2021). Developing a Modeling Framework to Simulate Compound Flooding: When Storm Surge Interacts With Riverine Flow. Frontiers in Climate, 2(February). https://doi.org/10.3389/fclim.2020.609610

Luettich, R.A., & Westerink, J. J. (1995a). *An assessment of flooding and drying techniques for use in the ADCIRC hydrodynamic model: Implementation and performance in one-dimensional flows*. *Report,US Army Corps of Engineers, Vicksburg, MSUS Army Corps of Engineers, Vicksburg, MS*.

Luettich, R.A., & Westerink, J. J. (1995b). *Implementation and testing of elemental flooding and drying in the ADCIRC hydrodynamic model*. *Report,US Army Corps of Engineers, Vicksburg, MSUS Army Corps of Engineers, Vicksburg, MS*.

Luettich, Richard A., Westerink, J. J., & Scheffner, N. W. (1992). *ADCIRC: An Advanced Three-Dimensional Circulation Model for Shelves, Coasts, and Estuaries. Report 1. Theory and Methodology of ADCIRC-2DDI and ADCIRC-3DL*. Vicksburg, MS.

Mahgerefteh, H., Rykov, Y., & Denton, G. (2009). Courant, Friedrichs and Lewy (CFL) impact on numerical convergence of highly transient flows. *Chemical Engineering Science*, *64*(23), 4969–4975. https://doi.org/10.1016/j.ces.2009.08.002

Mattocks, C., & Forbes, C. (2008). A real-time, event-triggered storm surge forecasting system for the state of North Carolina. *Ocean Modelling*, *25*(3–4), 95–119. https://doi.org/10.1016/j.ocemod.2008.06.008

1203 Mayo, T., Butler, T., Dawson, C., & Hoteit, I. (2014). Data assimilation within the Advanced Circulation (ADCIRC)
1204 modeling framework for the estimation of Manning ' s friction coefficient. *Ocean Modeling,* 76, 43–58.
1205 https://doi.org/10.1016/j.ocemod.2014.01.001
1206 Medeiros, S. C., & Hagen, Scott. C. (2012). Review of wetting and drying algorithms for numerical tidal flow
1207 models. *International Journal for Numerical Methods in Fluids*, *71*(4), 473–487. https://doi.org/10.1002/fld
1208 Moftakhari, H., Schubert, J. E., AghaKouchak, A., Matthew, R. A., & Sanders, B. F. (2019). Linking statistical and
1209 hydrodynamic modeling for compound flood hazard assessment in tidal channels and estuaries. Advances in
1210 Water Resources, 128(April), 28–38. https://doi.org/10.1016/j.advwatres.2019.04.009
1211 Mohanty, M. P., Sherly, M. A., Ghosh, S., & Karmakar, S. (2020). Tide-rainfall flood quotient: An incisive measure
1212 of comprehending a region's response to storm-tide and pluvial flooding. *Environmental Research Letters*,
1213 *15*(6). https://doi.org/10.1088/1748-9326/ab8092
1214 Moussa, R., & Bocquillon, C. (1996). Criteria for the choice of flood-routing methods in natural channels. *Journal*
1215 *of Hydrology*, *186*(1–4), 1–30. https://doi.org/10.1016/S0022-1694(96)03045-4
1216 NOAA. (2013). *National coastal population report: Population trends from 1970 to 2010*. *NOAA State of the Coast*
1217 *Report Series*.
1218 NOAA. (2016). NOAA Coastal Change Analysis Program (C-CAP) Regional Land Cover Database. Retrieved June
1219 2, 2021, from coast.noaa.gov/landcover
1220 NOAA. (2021). Tides and Currents. Retrieved from https://tidesandcurrents.noaa.gov/
1221 Orton, P. M., Conticello, F. R., Cioffi, F., Hall, T. M., Georgas, N., Lall, U., et al. (2018). Flood hazard assessment
1222 from storm tides, rain and sea level rise for a tidal river estuary. *Natural Hazards*, 1–29.
1223 https://doi.org/10.1007/s11069-018-3251-x
1224 Pandey, S., & Rao, A. D. (2019). Impact of Approach Angle of an Impinging Cyclone on Generation of Storm
1225 Surges and Its Interaction with Tides and Wind Waves. Journal of Geophysical Research : Oceans, 124, 7643–
1226 7660. https://doi.org/10.1029/2019JC015433
1227 Pugh, D., & Woodworth, P. (2014). Tidal analysis and prediction. In *Sea-Level Science: Understanding Tides,*
1228 *Surges, Tsunamis and Mean Sea-Level Changes* (pp. 60–96). Cambridge, UK: Cambridge University Press.
1229 https://doi.org/10.1017/CBO9781139235778
1230 Ray, T., Stepinski, E., Sebastian, A., & Bedient, P. B. (2011). Dynamic Modeling of Storm Surge and Inland
1231 Flooding in a Texas Coastal Floodplain. *Journal of Hydraulic Engineering*, *137*(10), 1103–1111.
1232 https://doi.org/10.1061/(ASCE)HY.1943-7900.0000398.
1233 Reddy, K. V., Eldho, T. I., Rao, E. P., & Hengade, N. (2007). A kinematic-wave-based distributed watershed model
1234 using FEM, GIS and remotely sensed data. *Hydrological Processes*, *21*, 2765–2777.
1235 https://doi.org/10.1002/hyp.6490
1236 Roberts, H. J., & Cobell, Z. (2017). 2017 Coastal Master Plan: Attachment C3-25.1: Storm SurgeRep. Baton Rouge,
1237 LA.
1238 Saleh, F., Ramaswamy, V., Wang, Y., Georgas, N., Blumberg, A., & Pullen, J. (2017). A multi-scale ensemble-
1239 based framework for forecasting compound coastal-riverine flooding: The Hackensack-Passaic watershed and
1240 Newark Bay. *Advances in Water Resources*, *110*, 371–386. https://doi.org/10.1016/j.advwatres.2017.10.026
1241 Santiago-Collazo, Félix L, Silva Araya, W. F., González López, J., & Maldonado, J. M. (2017). Flooding Effects
1242 Combining Storm Surge and Surface Runoff during Hurricane Georges on the Eastern Coast of Puerto Rico.
1243 *Revista Internacional de Desastres Naturales, Accidentes e Infraestructura Civil*, *17*(2), 45–71. Retrieved
1244 from ttps://www.scipedia.com/public/Santiago-Collazo_et_al_2017a
1245 Santiago-Collazo, Félix L., Bilskie, M. v., & Hagen, S. C. (2019). A comprehensive review of compound inundation
1246 models in low-gradient coastal watersheds. *Environmental Modelling & Software*, *119*, 166–181.
1247 https://doi.org/10.1016/j.envsoft.2019.06.002
1248 Santiago-Collazo, Félix L, Bilskie, M. V, Bacopoulos, P., & Hagen, Scott. C. (2021a). An Examination of
1249 Compound Flood Hazard Zones for Past , Present , and Future Low-Gradient Coastal. *Frontiers in Climate*, *3*,
1250 1–19. https://doi.org/10.3389/fclim.2021.684035
1251 Santiago-Collazo, F. L, Bilskie, M. v, Bacopoulos, P., & Hagen, S. C. (2021b). Maximum water level profiles for
1252 each simulation under each flooding scenario. [Dataset]. Figshare.
1253 https://figshare.com/s/23585d5d4ed005941ab2
1254 Santiago-Collazo, F.L, Bilskie, M. v, Bacopoulos, P., & Hagen, S. C. (2021c). Time to peak water levels profiles for
1255 each simulation under each flooding scenario. [Dataset]. Figshare.
1256 https://figshare.com/s/3d526bb47932627dce54

1257 Santiago-Collazo, F.L, Bilskie, M. v, Bacopoulos, P., & Hagen, Scott. C. (2021d). Combinations of the
1258 environmental forcing parameters created using the Random Sampling Technique. [Dataset]. Figshare.
1259 https://figshare.com/s/3d526bb47932627dce54
1260 Santiago-Collazo, F., Bilskie, Matthew, Bacopoulos, Peter, & Hagen, Scott. (2023). 1D Shallow Water Equation
1261 Model for Rainfall-Runoff and Coastal Processes (v.1.0.0). [Software]. Zenodo.
1262 https://doi.org/10.5281/zenodo.8121074
1263 Santiago-Collazo, F.L., & Silva-Araya, W. F. (2019). Computational Model for Gradually Varied Flow in Channel
1264 Networks with Hydraulic Structures. *Journal of Irrigation and Drainage Engineering*, *145*(6), 1–13.
1265 https://doi.org/10.1061/(ASCE)IR.1943-4774.000138
1266 Serafin, K. A., Ruggiero, P., Parker, K. A., & Hill, D. F. (2019). What ' s streamflow got to do with it ? A
1267 probabilistic simulation of the competing oceanographic and fluvial processes driving extreme along-river
1268 water levels. Natural Hazards and Earth System Science Discussions, (January). https://doi.org/10.5194/nhess-
1269 2018-347
1270 Shen, Y., Morsy, M. M., Huxley, C., Tahvildari, N., & Goodall, J. L. (2019). Flood risk assessment and increased
1271 resilience for coastal urban watersheds under the combined impact of storm tide and heavy rainfall. *Journal of*
1272 *Hydrology*, *579*(September), 124159. https://doi.org/10.1016/j.jhydrol.2019.124159
1273 Silva-Araya, W., Santiago-Collazo, F., Gonzalez-Lopez, J., & Maldonado-Maldonado, J. (2018). Dynamic
1274 Modeling of Surface Runoff and Storm Surge during Hurricane and Tropical Storm Events. *Hydrology*, *5*(1),
1275 13. https://doi.org/10.3390/hydrology5010013
1276 Singh, Vijay P. (1996). *Kinematic Wave Modeling in Water Resources: Surface Water Hydrology*. New York, NY:
1277 John Wiley & Sons, Inc.
1278 Singh, V. P. (2002). Is hydrology kinematic? *Hydrological Processes*, *16*(3), 667–716.
1279 https://doi.org/10.1002/hyp.306
1280 Tang, H. S., Chien, S. I. J., Temimi, M., Blain, C. A., Ke, Q., Zhao, L., & Kraatz, S. (2013). Vulnerability of
1281 population and transportation infrastructure at the east bank of Delaware Bay due to coastal flooding in sea-
1282 level rise conditions. *Natural Hazards*, *69*(1), 141–163. https://doi.org/10.1007/s11069-013-0691-1
1283 Tehranirad, B., Herdman, L., Nederhoff, K., Erikson, L., Cifelli, R., Pratt, G., et al. (2020). Effect of fluvial
1284 discharges and remote non-tidal residuals on compound flood forecasting in San Francisco Bay. *Water*
1285 *(Switzerland)*, *12*(9). https://doi.org/10.3390/w12092481
1286 Terry, J. P., Winspear, N., & Goff, J. (2021). Is Bangkok at risk of marine flooding? Evidence relating to the
1287 historical floods of AD 1785 and 1983. *Natural Hazards*, *105*(1), 1013–1030. https://doi.org/10.1007/s11069-
1288 020-04347-4
1289 Torres, J. M., Bass, B., Irza, N., Fang, Z., Proft, J., Dawson, C., et al. (2015). Characterizing the hydraulic
1290 interactions of hurricane storm surge and rainfall-runoff for the Houston-Galveston region. *Coastal*
1291 *Engineering*, *106*, 7–19. https://doi.org/10.1016/j.coastaleng.2015.09.004
1292 Veeramony, J., & Blain, C. A. (2001). Barotropic Flow in the Vicinity of an Idealized Inlet — Simulations with the
1293 ADCIRC model. Naval Research Laboratory, Washington, DC.
1294 Wahl, T., Jain, S., Bender, J., Meyers, S. D., & Luther, M. E. (2015). Increasing risk of compound flooding from
1295 storm surge and rainfall for major US cities. *Nature Climate Change*, *5*, 1093–1098.
1296 https://doi.org/10.1038/nclimate2736
1297 Wang, H., Loftis, J., Liu, Z., Forrest, D., & Zhang, J. (2014). The Storm Surge and Sub-Grid Inundation Modeling
1298 in New York City during Hurricane Sandy. *Journal of Marine Science and Engineering*, *2*(1), 226–246.
1299 https://doi.org/10.3390/jmse2010226
1300 Ward, P. J., Couasnon, A., Eilander, D., Haigh, I. D., Hendry, A., Muis, S., et al. (2018). Dependence between high
1301 sea-level and high river discharge increases flood hazard in global deltas and estuaries. Environmental
1302 Research Letters, 13, 1–12. https://doi.org/10.1088/1748-9326/aad400
1303 West, D. W., Kubatko, E. J., Conroy, C. J., Yaufman, M., & Wood, D. (2017). A multidimensional discontinuous
1304 Galerkin modeling framework for overland flow and channel routing. *Advances in Water Resources*, *102*,
1305 142–160. https://doi.org/10.1016/j.advwatres.2017.02.008
1306 Westerink, J. J., Luettich, R. A., Feyen, J. C., Atkinson, J. H., Dawson, C., Roberts, H. J., et al. (2008). A Basin- to
1307 Channel-Scale Unstructured Grid Hurricane Storm Surge Model Applied to Southern Louisiana. *Monthly*
1308 *Weather Review*, *136*(3), 833–864. https://doi.org/10.1175/2007MWR1946.1
1309 Xu, K., Wang, C., & Bin, L. (2023). Compound flood models in coastal areas : a review of methods and uncertainty
1310 analysis. Natural Hazards, 116(1), 469–496. https://doi.org/10.1007/s11069-022-05683-3
1311 Xu, S., & Huang, W. (2014). An improved empirical equation for storm surge hydrographs in the Gulf of Mexico,
1312 U.S.A. *Ocean Engineering*, *75*, 174–179. https://doi.org/10.1016/j.oceaneng.2013.11.004

Ye, F., Zhang, Y. J., Yu, H., Sun, W., Moghimi, S., Myers, E., et al. (2020). Simulating storm surge and compound flooding events with a creek-to-ocean model: Importance of baroclinic effects. *Ocean Modelling*, *145*(September 2019), 101526. https://doi.org/10.1016/j.ocemod.2019.101526

Yin, D., Muñoz, D. F., Bakhtyar, R., Xue, Z. G., Moftakhari, H., Ferreira, C., & Mandli, K. (2021). Extreme Water Level Simulation and Component Analysis in Delaware Estuary during Hurricane Isabel. *Journal of the American Water Resources Association*. https://doi.org/10.1111/1752-1688.12947

Zhang, Y., & Najafi, M. R. (2020). Probabilistic Numerical Modeling of Compound Flooding Caused by Tropical Storm Matthew Over a Data-Scarce Coastal Environment. *Water Resources Research*, *56*(10). https://doi.org/10.1029/2020WR028565

Zhang, Y. J., Ye, F., Yu, H., Sun, W., Moghimi, S., Myers, E., et al. (2020). Simulating compound flooding events in a hurricane. *Ocean Dynamics*, *70*(5), 621–640. https://doi.org/10.1007/s10236-020-01351-x

Figure 1.

A

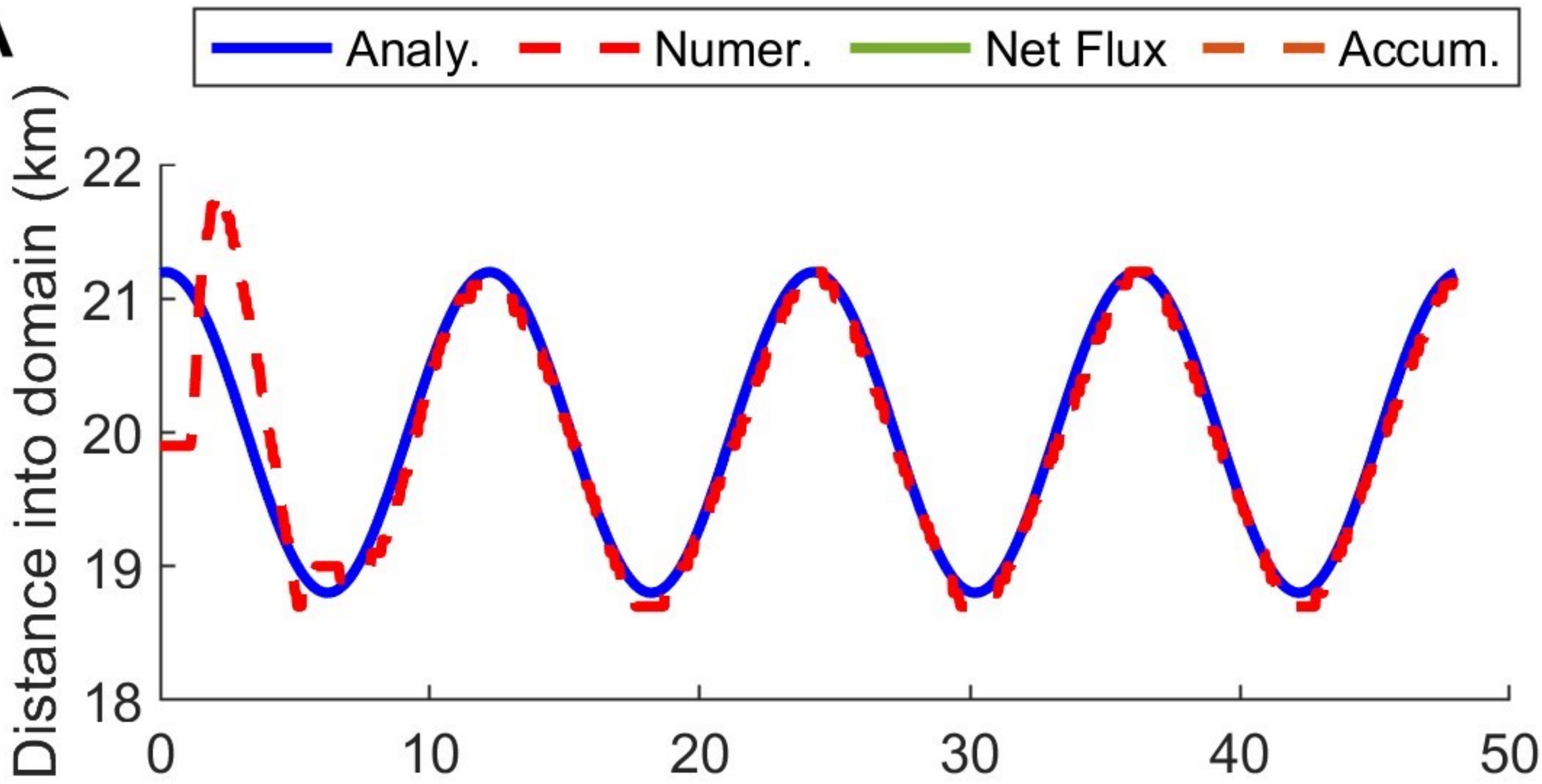
Analy.
Numer.
Net Flux
Accum.
Distance into domain (km)
22
21
20
19
18
0
10
20
30
40
50
Time (hr)

B

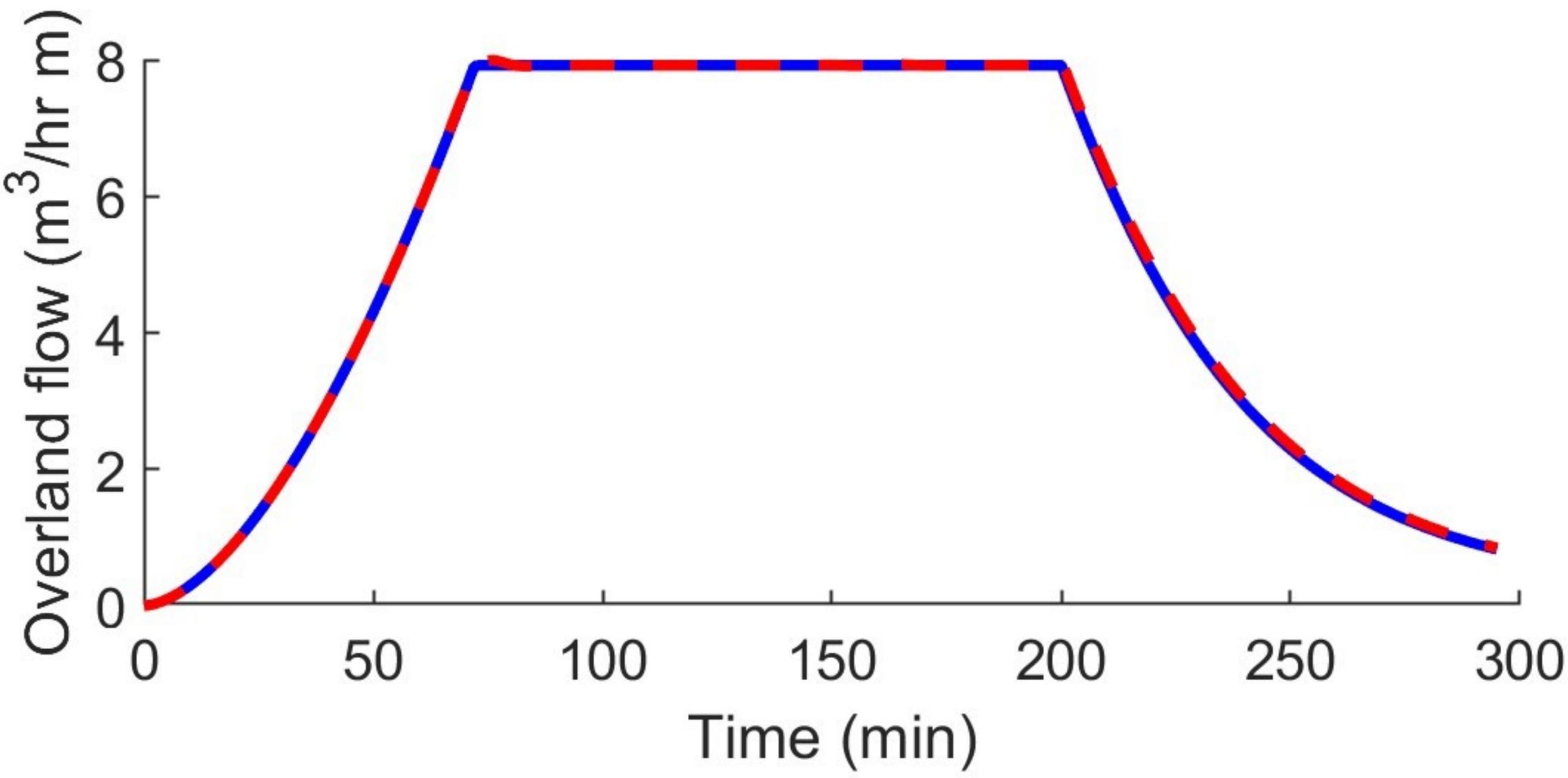
Overland flow (m3/hr m)
8
6
4
2
0
0
50
100
150
200
250
300
Time (min)

C

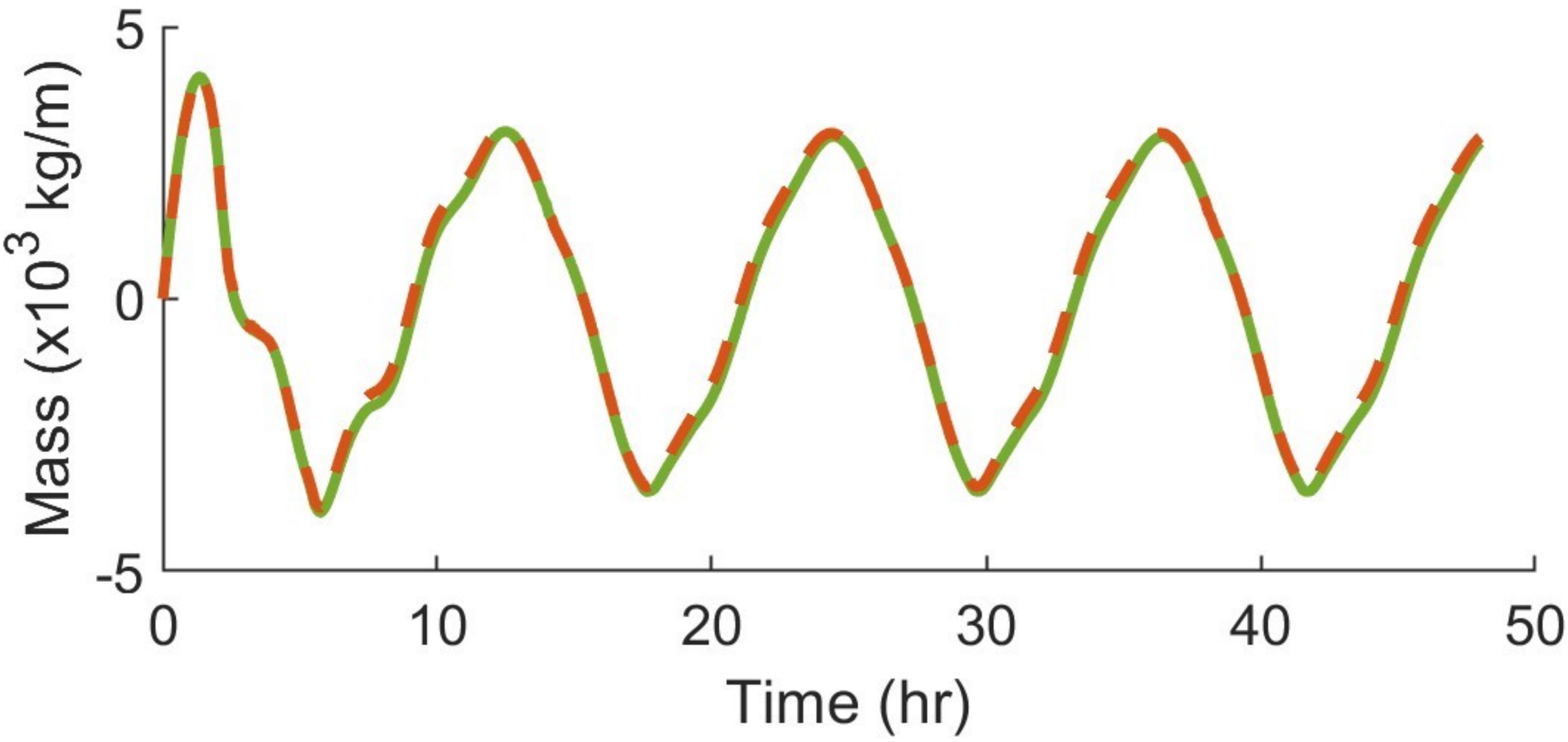
Mass (x10^3 kg/m)
5
0
-5
0
10
20
30
40
50
Time (hr)

Figure 2.

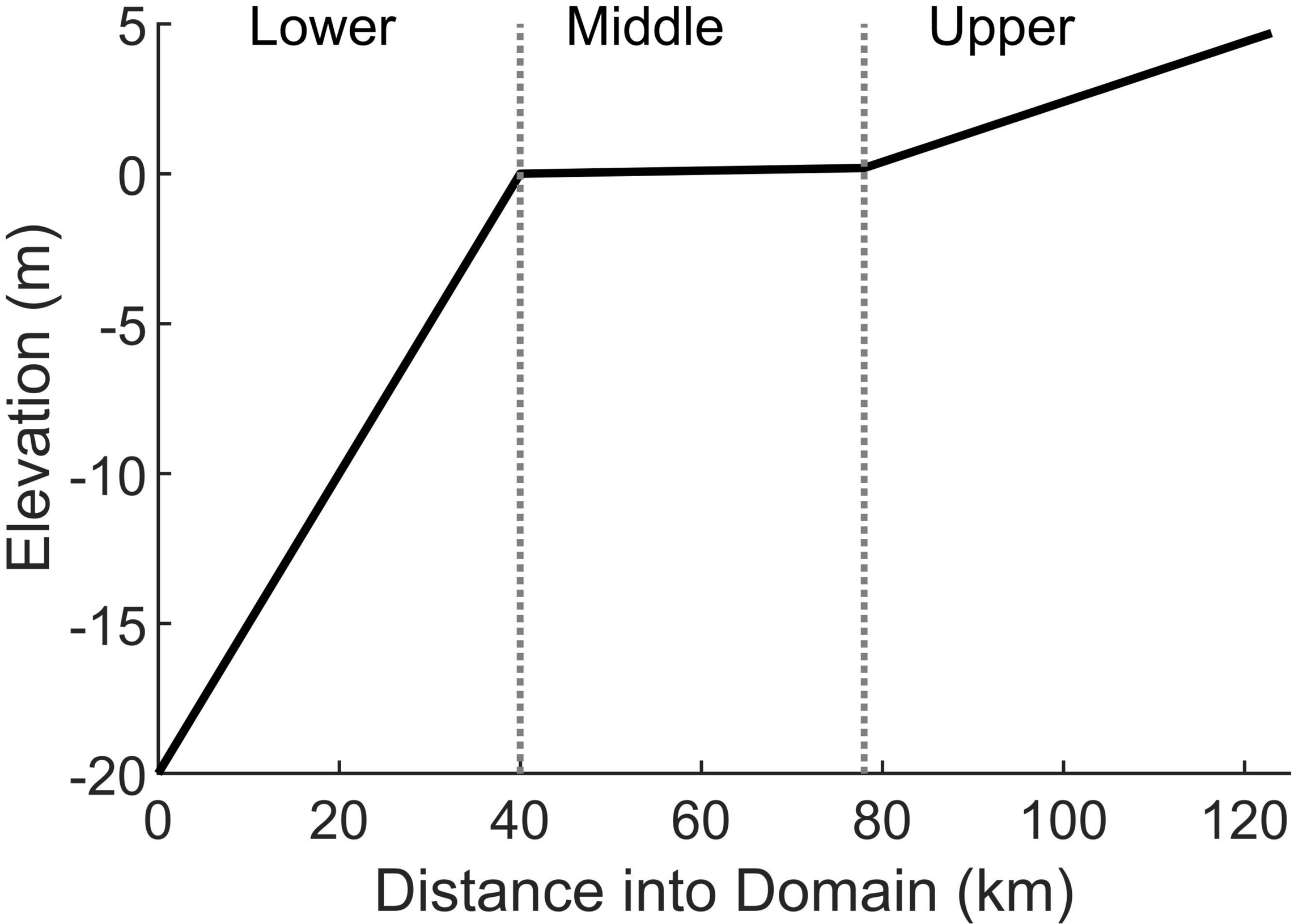
Lower
Middle
Upper
5
0
-5
-10
-15
-20
Elevation (m)
0
20
40
60
80
100
120
Distance into Domain (km)

Figure 3.

S R RS Bottom Change in Slope

A

26-hr

Elevation (m)

B

26-hr

Flow (m^3/s m)

C

54-hr

Elevation (m)

D

54-hr

Flow (m^3/s m)

E

64-hr

Elevation (m)

Distance into domain (km)

F

64-hr

Flow (m^3/s m)

Distance into domain (km)

Figure 4.

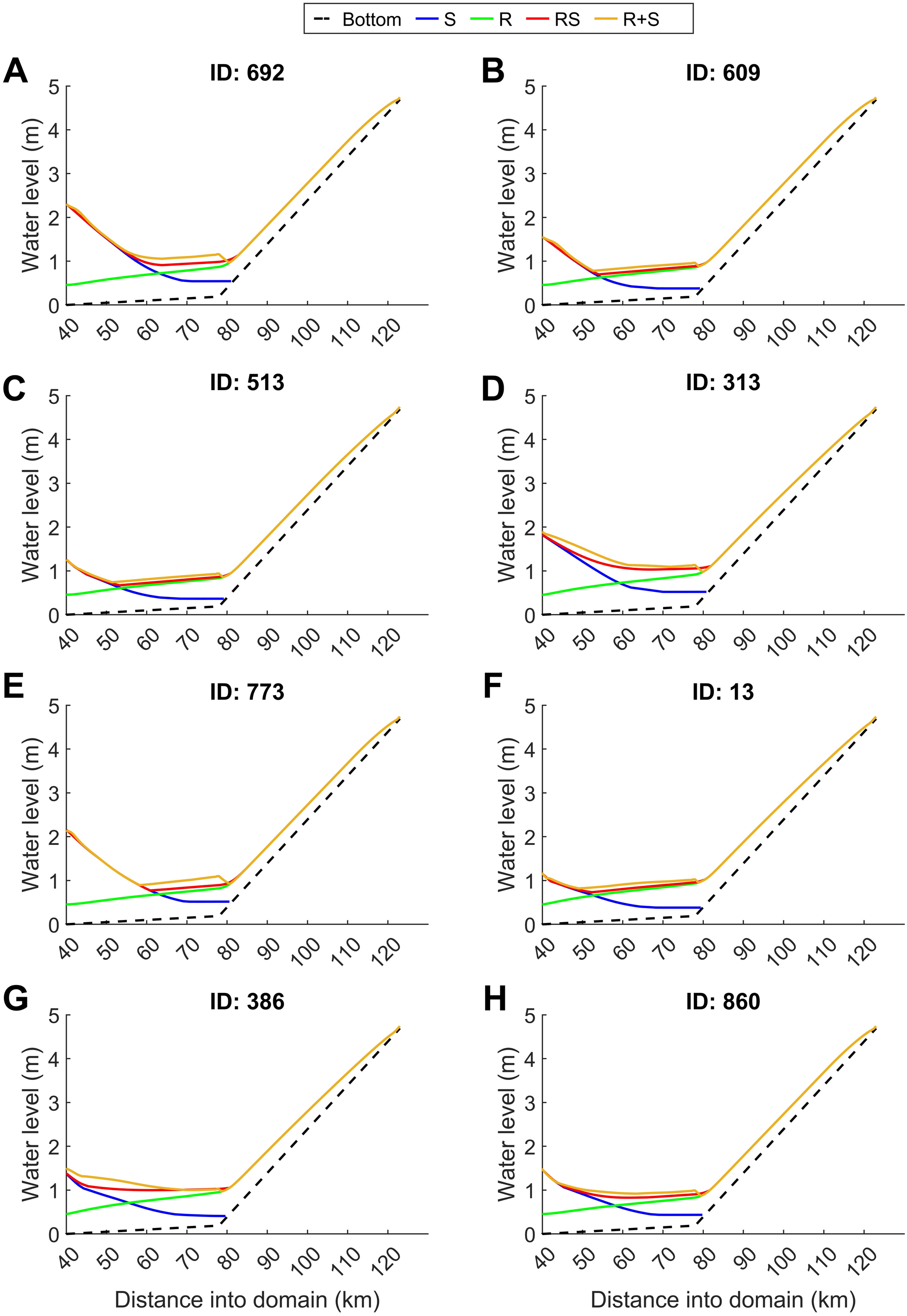
Bottom
S
R
RS
R+S
A
ID: 692
B
ID: 609
C
ID: 513
D
ID: 313
E
ID: 773
F
ID: 13
G
ID: 386
H
ID: 860
Water level (m)
Distance into domain (km)
0
1
2
3
4
5
40
50
60
70
80
90
100
110
120

Figure 5.

S R RS

A

ID: 692

B

ID: 609

C

ID: 513

D

ID: 313

E

ID: 773

F

ID: 13

G

ID: 386

H

ID: 860

Time to peak water level (hr)

Distance into domain (km)

Figure 6.

A

B

C

D

E

F

Mean
+/- Std Dev
Min/Max
Bottom

Water level (m)

Time to peak water level (hr)

Distance into Domain (km)

Figure 7.

A

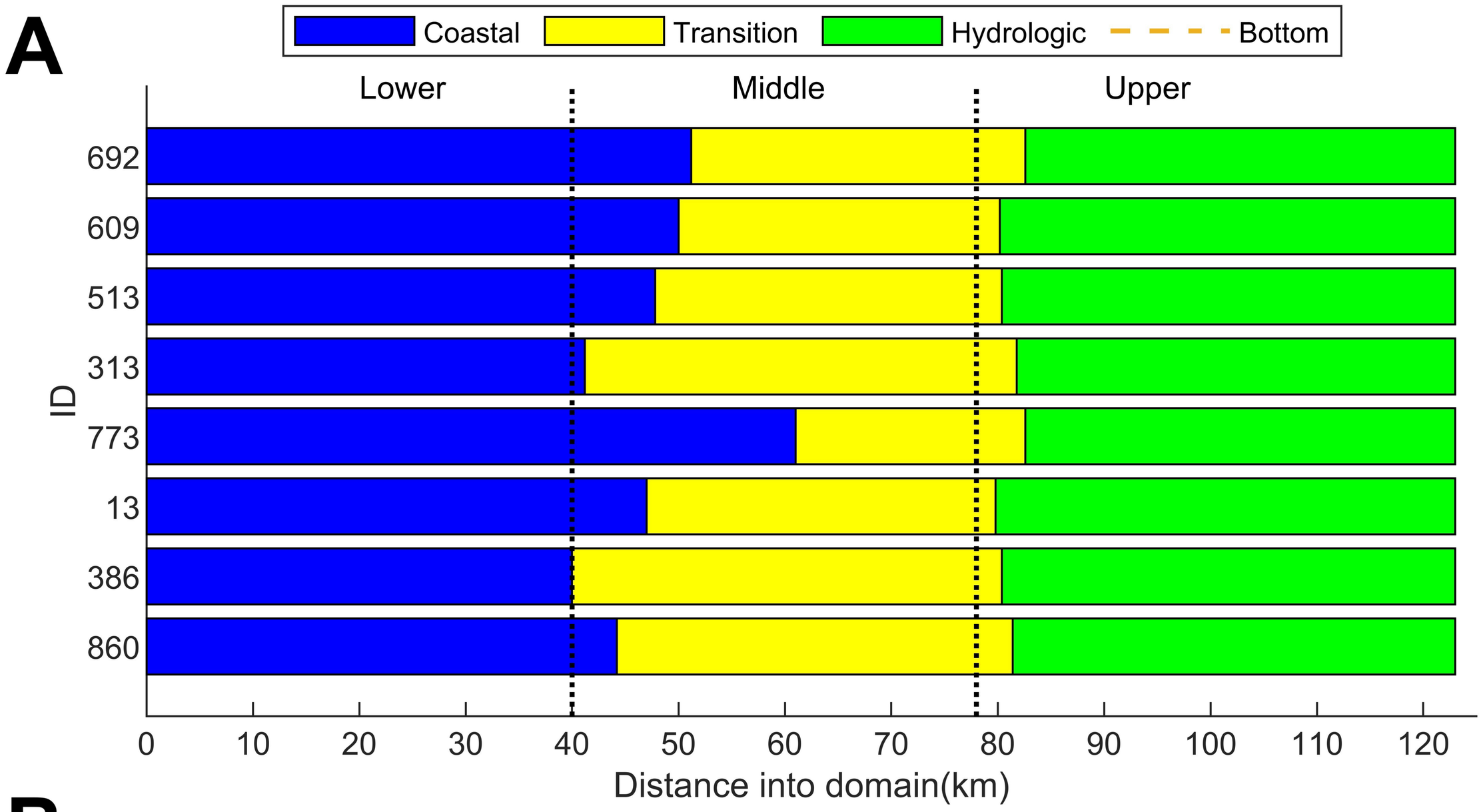
Coastal
Transition
Hydrologic
Bottom
Lower
Middle
Upper
692
609
513
313
773
13
386
860
ID
0
10
20
30
40
50
60
70
80
90
100
110
120
Distance into domain(km)

B

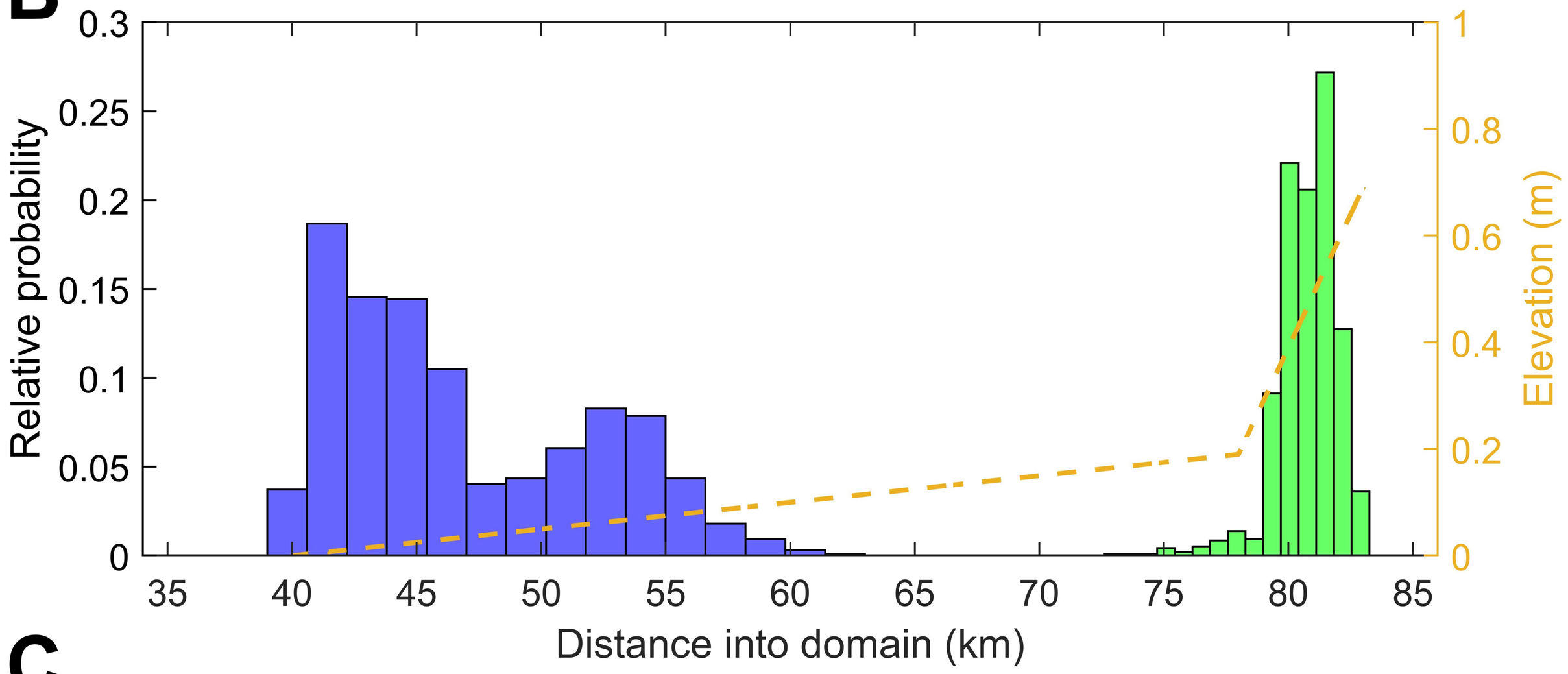
Relative probability
0.3
0.25
0.2
0.15
0.1
0.05
0
1
0.8
0.6
0.4
0.2
0
Elevation (m)
35
40
45
50
55
60
65
70
75
80
85
Distance into domain (km)

C

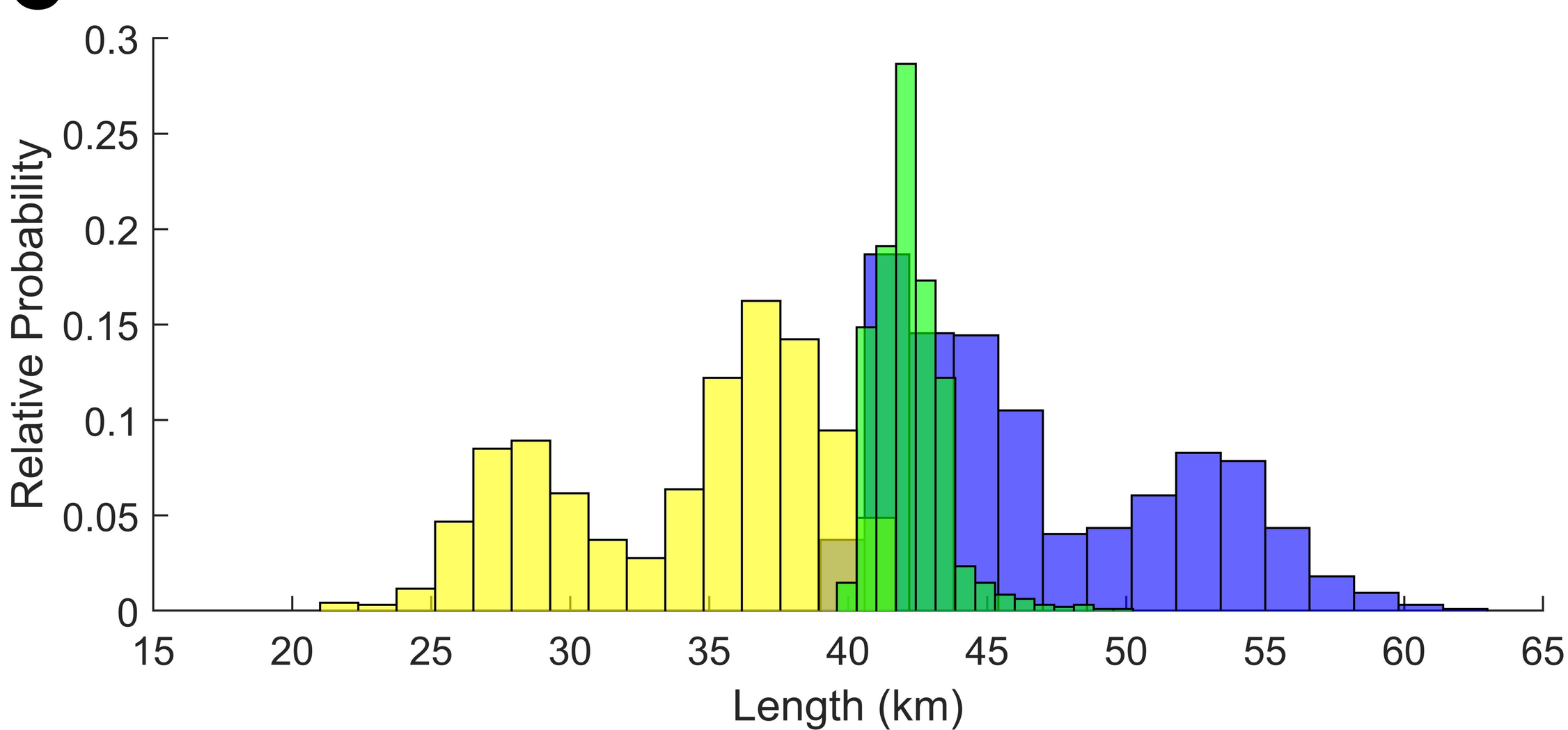
Relative Probability
0.3
0.25
0.2
0.15
0.1
0.05
0
15
20
25
30
35
40
45
50
55
60
65
Length (km)

Figure 8.

A

Complete

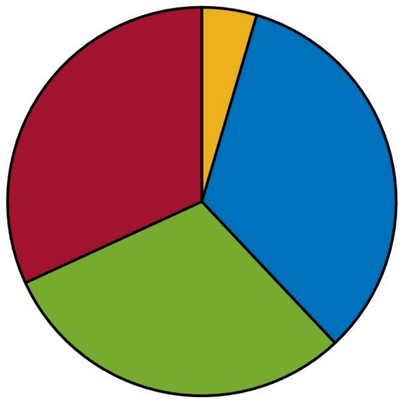

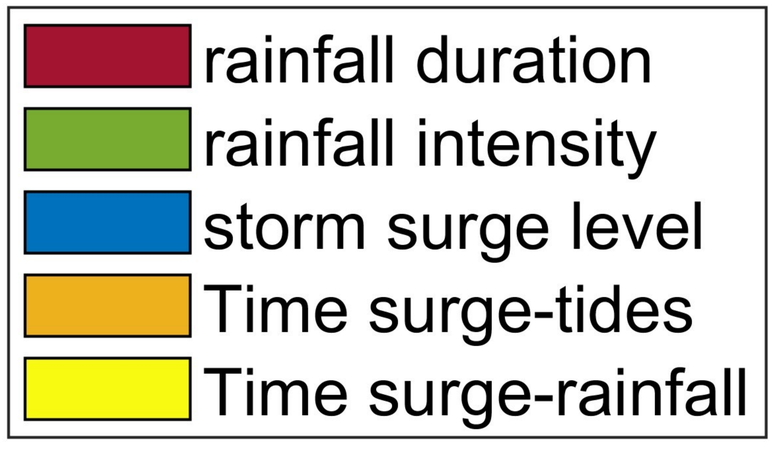

B

Lower

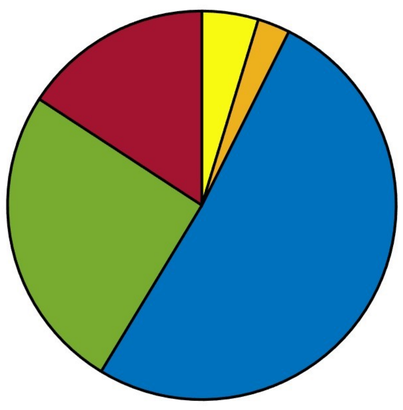

C

Coastal

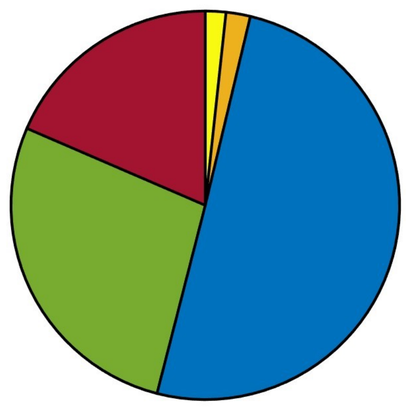

D

Middle

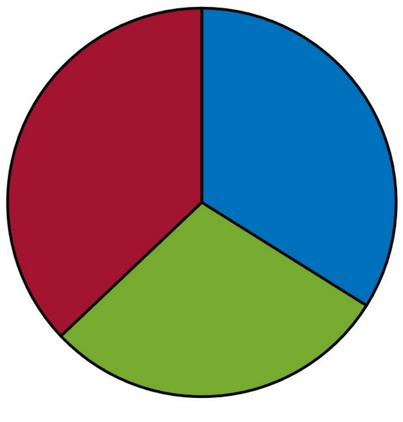

E

Transition

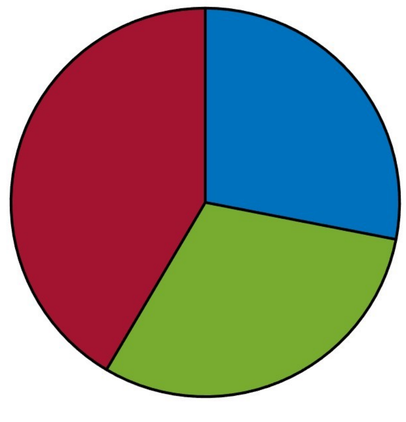

F

Upper

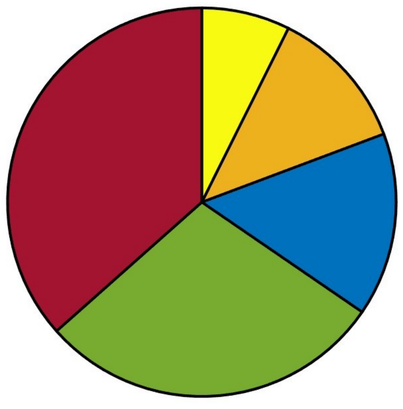

G
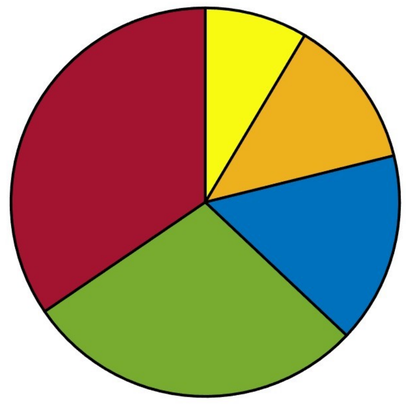
Hydrologic